" EQUIVALENT CIRCUIT MODELS FOR HYSTERESIS MOTOR".

A
THESIS
SUBMITTED
TO THE DEPARTMENT
OF ELECTRICAL ENGINEERING
BANGLADESH UNIVERSITY OF ENGINEERING
& TECHNOLOGY,DACCA, IN PARTIAL FULFILMENT OF
THE REQUIREMENTS FOR THE DEGREE OF MASTER
OF SCIENCE (ENGINEERING) IN ELECTRICAL ENGINEERING.

BY
NIRANJAN CHANDRA BHAKTA

DEPARTMENT OF ELECTRICAL ENGINEERING
BANGLADESH UNIVERSITY OF ENGINEERING
AND TECHNOLOGY, DACCA.
1973

C E R T I F I C A T E

THIS IS TO CERTIFY THAT THIS WORK WAS DONE BY ME AND IT HAS NOT BEEN SUBMITTED ELSEWHERE FOR THE AWARD OF ANY DEGREE OR DIPLOMA OR FOR PUBLICATION.

Countersigned

m Rehman
.....
Supervisor

Niranjan Chandra Bhakta
Signature of the Candidate

ACCEPTED AS SATISFACTORY FOR PARTIAL FULFILMENT OF THE REQUIREMENTS FOR THE DEGREE OF M.Sc. (ENGINEERING) IN ELECTRICAL ENGINEERING.

EXAMINERS :

(i) ..... June 23, 1973

(ii) .....

(iii) .....

(iv) .....

ACKNOWLEDGEMENT

THE AUTHOR WISHES TO ACKNOWLEDGE HIS INDEBTEDNESS TO ASSOCIATE PROFESSOR, DR. M.A.RAHMAN, FOR SUGGESTING THE PROBLEM, FOR GUIDANCE, AND FOR CONSTANT ENCOURAGEMENT IN THE COURSE OF THE WORK, AND FOR DEMONSTRATION AS TO HOW TO FIT THE ELEMENTS IN THE EQUIVALENT CIRCUIT MODELS, AND TO GET THE ANALYTICAL SOLUTIONS.

THE AUTHOR ALSO WISHES TO GRATEFULLY ACKNOWLEDGE THE ASSISTANCE FROM THE DEPARTMENT OF ELECTRICAL ENGINEERING, BANGLADESH UNIVERSITY OF ENGINEERING AND TECHNOLOGY FOR PROVIDING SUCH FACILITIES OF RESEARCH WORK.

THE AUTHOR ALSO WISHES TO EXPRESS HIS DEEP SENSE OF APPRECIATION TO POWER DEVELOPMENT BOARD AUTHORITY FOR GIVING PERMISSION TO PERFORM THIS WORK.

THE AUTHOR ALSO GRATEFULLY ACKNOWLEDGE THE ENCOURAGEMENT FROM MR. SHAMSUL HUDA, EX-DIRECTOR, PROGRAMME, MR.SHAMSUL ISLAM, DIRECTOR, PROGRAMME, MR.S.T.S.MAHMOOD, DY.DIRECTOR, DESIGN, POWER DEVELOPMENT BOARD IN THIS WORK.

THE ASSISTANCE FROM MR.JOHN COSTA, TYPIST, MR.SHARIF MOLLAH, DAFTORY OF DIRECTORATE OF PROGRAMME AND MR.JIBAN CHANDRA SUTRADHAR, DRAFTSMAN OF DIRECTORATE OF PLANNING, POWER DEVELOPMENT BOARD IN TYPING, SKETCHING AND PRINTING IS THANKFULLY ACKNOWLEDGED.

ABSTRACT

Using parallelogram model to the B-H characteristic of the hysteresis material, general expressions for the terminal quantities of a circumferential flux polyphase hysteresis machine are derived. A detail analysis of the phenomena of parasitic losses, stator iron loss and saturation in stator core is made.

General equivalent circuit models for polyphase hysteresis motors for both synchronous and sub-synchronous mode of operation are developed. Modified equialent circuit models are also developed for both the cases.

The effect of saturation in stator core,parasitic losses and stator iron loss are represented by suitable parameters in the general equivalent circuit models.

Analytical solutions of the equivalent circuit models are made for balanced polyphase hysteresis motors. The equivalent circuit models are clearly expressed by phasor equations.

It is established that the machine torque at sub-synchronous speed is higher than the pull-out torque at synchronous speed and this additional torque at sub-synchronous speed is supplied by the eddy current torque. This is found to be in close agreement with that obtained experimentally.

GLOSSARY OF SYMBOLS

a_i - factor (eqn.23).

B - magnetic flux density.

$\hat{B}$ - peak of tooth ripple flux density.

$\bar{B}$ - peak of mean flux density in the airgap neglecting tooth ripple.

B_1 - fundamental component of airgap flux density.

$\bar{B}_1$ - peak of fundamental component of airgap flux density.

B_g - airgap flux density.

$\bar{B}_g$ - peak of airgap flux density.

$B_{g\theta}$ - airgap flux density at angle θ .

$B_{h\theta}$ - circumferential flux density in hysteresis material at angle θ .

$\hat{B}_i$ - peak of ith component of tooth ripple flux density.

B_r - residual flux density.

B_t - radially directed stator tooth leakage flux density.

B_{tip} - tip-to-tip circumferential leakage flux density.

d - effective radial depth of slot leakage flux path.

E - voltage.

E_g - per phase airgap voltage.

E_p - equivalent voltage of the idealized hysteresis element.

E_r - rotor induced voltage.

E_s - per phase stator supply voltage.

F - general symbol for magnetic potential.

F_{θ} - total magnetic potential at angle θ .

$F_{g\theta}$ - magnetic potential drop in airgap at angle θ .

$F_{h\theta}$ - magnetic potential drop in hysteresis material at angle θ .

$F_{o\theta}$ - magnetic potential drop across R_o .

$F_{p\theta}$ - magnetic potential drop across R_p .

$F_{q\theta}$ - Thevenin equivalent magnetic potential.

f - frequency.

f_1 - frequency of the fundamental component.

f_n - frequency of the nth harmonic.

f_r - induced rotor frequency.

f_t - tooth ripple frequency.

g - airgap.

g_e - carter equivalent airgap.

H - magnetic field intensity.

H_c - coercive force.

$H_{h\theta}$ - magnetic field intensity in hysteresis material at angle θ .

h - thickness of rotor hysteresis ring.

i - order of harmonics.

i_a - instantaneous stator current per phase.

I_c - current in eddy element.

I_f - current in flux parasitic element.

I_g - current through L_g .

I_{go} - current through jX_{go} .

I_h - current in hysteresis element.

I_i - current in iron loss element.

I_o - current through L_o .

I_p - current through jX_p .

I_s - r.m.s. stator current.

$\bar{I}_s$ - peak of stator current.

I_{ty} - current through jX_{ty} .

J - factor expressing fundamental solution of Fourier Series of flux space wave.

J_θ - stator current density.

K - constant.

K_d - stator winding distribution factor.

K_{dn} - stator winding distribution factor for nth harmonic.

K_f, K'_f - flux-parasitic loss constant.

K_m - mmf-parasitic loss constant.

K_{mn} - nth harmonic mmf-parasitic loss constant.

K_p - stator winding pitch factor.

K_{pn} - stator winding pitch factor for nth harmonic.

K_w - winding factor.

l - axial length of rotor.

L_g - inductance dual to $\mathcal{R}_{go}$.

L_{go} - parallel equivalent of L_g and L_o.

L_o - inductance dual to $\mathcal{R}_o$.

L_p - inductance dual to $\mathcal{R}_p$.

m - number of phase.

n - order of harmonic.

N_s - number of turns per phase.

P - number of poles.

P_c - per phase I^2R loss.

P_e - eddy current loss.

P_f - flux - parasitic loss.

P_h - hysteresis loss.

P_m - mmf - parasitic loss.

P_{mn} - mmf-parasitic loss for nth harmonic.

P_o - out put power per phase.

p - stator slot pitch.

$\mathcal{R}_{g\theta}$ - airgap reluctance per unit angle.

$\mathcal{R}_o$ - incremental reluctance per unit angle derived from slope of sides of $F - \phi$ loop.

$\mathcal{R}_p$ - incremental reluctance derived from $\mathcal{R}_s$ and $\mathcal{R}_o$.

$\mathcal{R}_s$ - incremental reluctance per unit angle derived from slope of top and bottom of $F - \phi$ loop.

R_e - equivalent resistance due to eddy current.

R_f - equivalent resistance due to flux-parasitic loss.

R_h - equivalent hysteresis resistance.

R_i - equivalent iron loss resistance.

R_m - equivalent resistance due to mmf-parasitic loss.

R_s - stator effective resistance per phase.

r - machine radius.

r_g - radius at airgap.

r_h - radius to centre of hysteresis ring.

S - slip.

S_1 - number of slots per pole.

s - slot width.

t - time.

t' - tooth width.

V - volume of rotor hysteresis ring.

W_h - hysteresis energy per unit volume.

X_g - reactance of L_g .

X_{go} - parallel equivalent of X_g and X_o .

X_o - reactance of L_o .

X_p - reactance of L_p .

X_r - rotor leakage reactance.

X_s - stator effective reactance per phase.

X_{sa} - stator end - winding reactance.

X_{sb} - stator slot, tooth-top and zigzag reactance.

X_{ty} - stator tooth-body and yoke reactance.

Z - number of conductors per phase per pole.

Greek symbols:

δ - torque angle.

μ - permeability of hysteresis material.

μ_o - permeability of free space.

μ_p - equivalent permeability from μ_{ro} and μ_{rs}.

μ_r - recoil permeability.

μ_{ro} - unsaturated relative permeability.

μ_{rs} - saturated relative permeability.

ϕ - flux.

ϕ_h - flux in the hysteresis ring.

ϕ_θ - flux at angle θ.

$\phi_{p\theta}$ - flux through non-linear element at angle θ.

ϕ_{tip} - tip-to-tip circumferential leakage flux.

ϕ_{my} - mutual flux in the yoke corresponding to fundamental component of airgap flux.

ϕ_{Ly} - yoke leakage flux.

θ - radial angle.

α - phase angle.

α_m - phase angle for ≅ zero power factor load.

w - angular speed.

χ - factor (eqn.16).

$\gamma, \gamma_n, \gamma_i$ - factor. (eqn.14).

β, β_n, β_i - factor,(eqn.15).

β' - angle between Thevenin equivalent magnetic potential $F_{q\theta}$ and ϕ_θ

λ - wave length.

ρ - resistivity of hysteresis material.

α - skin depth.

η_i - reduction factor (eqn.24).

L I S T _ O F _ F I G U R E S

TABLE OF CONTENTS

CHAPTER I

I. INTRODUCTION:

Hysteresis Machine is a torque producing device utilising the energy contained in the hysteresis loop of the rotor material. In this type of machine the stator is slotted and contains a sinusoidally distributed polyphase winding. The rotor contains no winding. It is made of an iron or aluminium core rounded by a ring of soft magnetic material. A uniform airgap is maintained throughout between the rotor and the stator. When a balanced set of sinusoidal currents is supplied to the stator winding, it produces a sinusoidally distributed magnetomotive force space wave revolving at synchronous speed around the airgap which causes a non-sinusoidal flux space wave. This flux crosses the airgap and enters the ring of soft magnet material of the rotor radially. The basic elements of a polyphase hysteresis machine is ullustrated in Fig. I.

Two types of concepts regarding the path of the flux in the rotor magnetic ring have been assumed so far. In the first type the flux crosses both the airgap and the rotor hysterèsis ring radially. This type of the hysteresis machine is known as radial - flux hysteresis machine as shown in Fig. 2a. In the other type, the flux crosses the airgap and enteres the hysteresis ring radially, and then passes through the hysteresis ring circumferentially. This type is called the circumferential - flux hysteresis machines as shown in Fig. 2b.

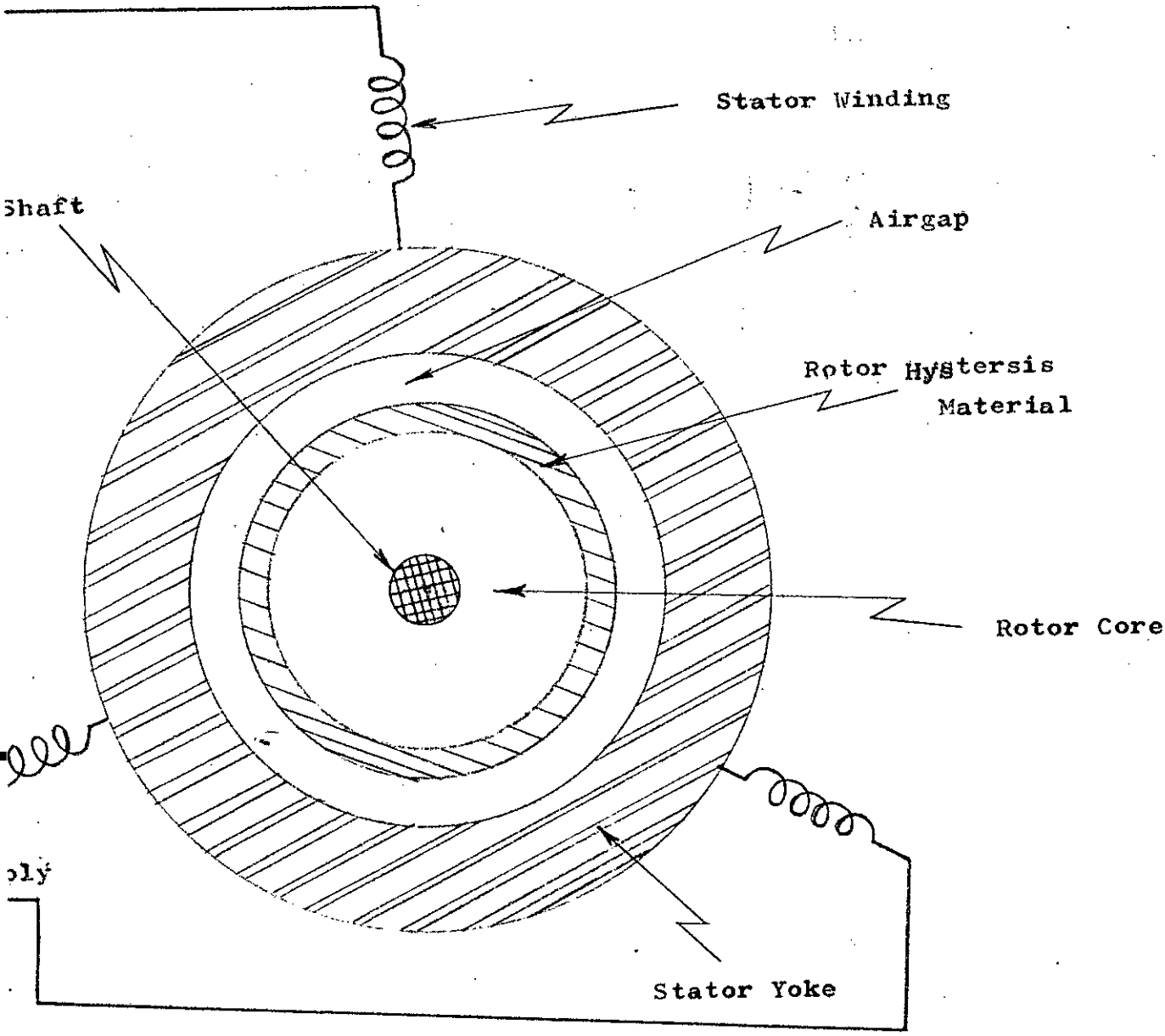

Fig.1. Schematic Representation of a Polyphase Hystersis Machine.

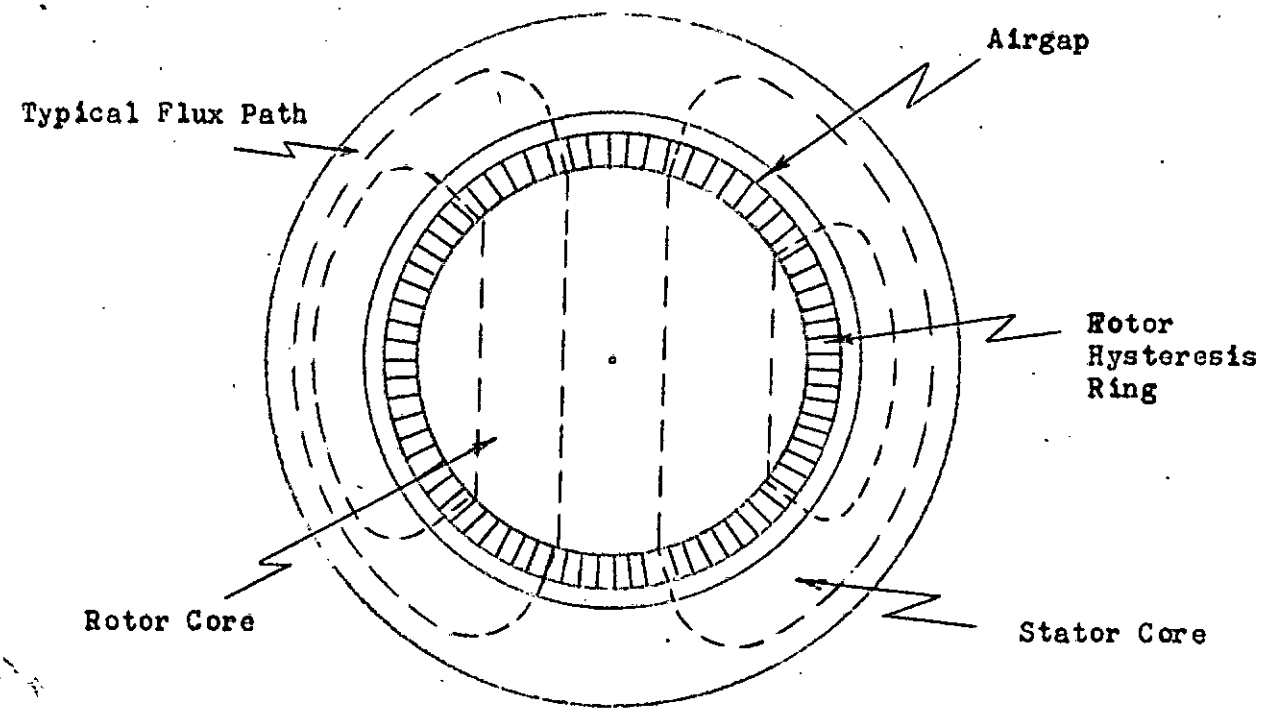

Fig.2aTypical Flux Path in Radial Flux Hysteresis Machine

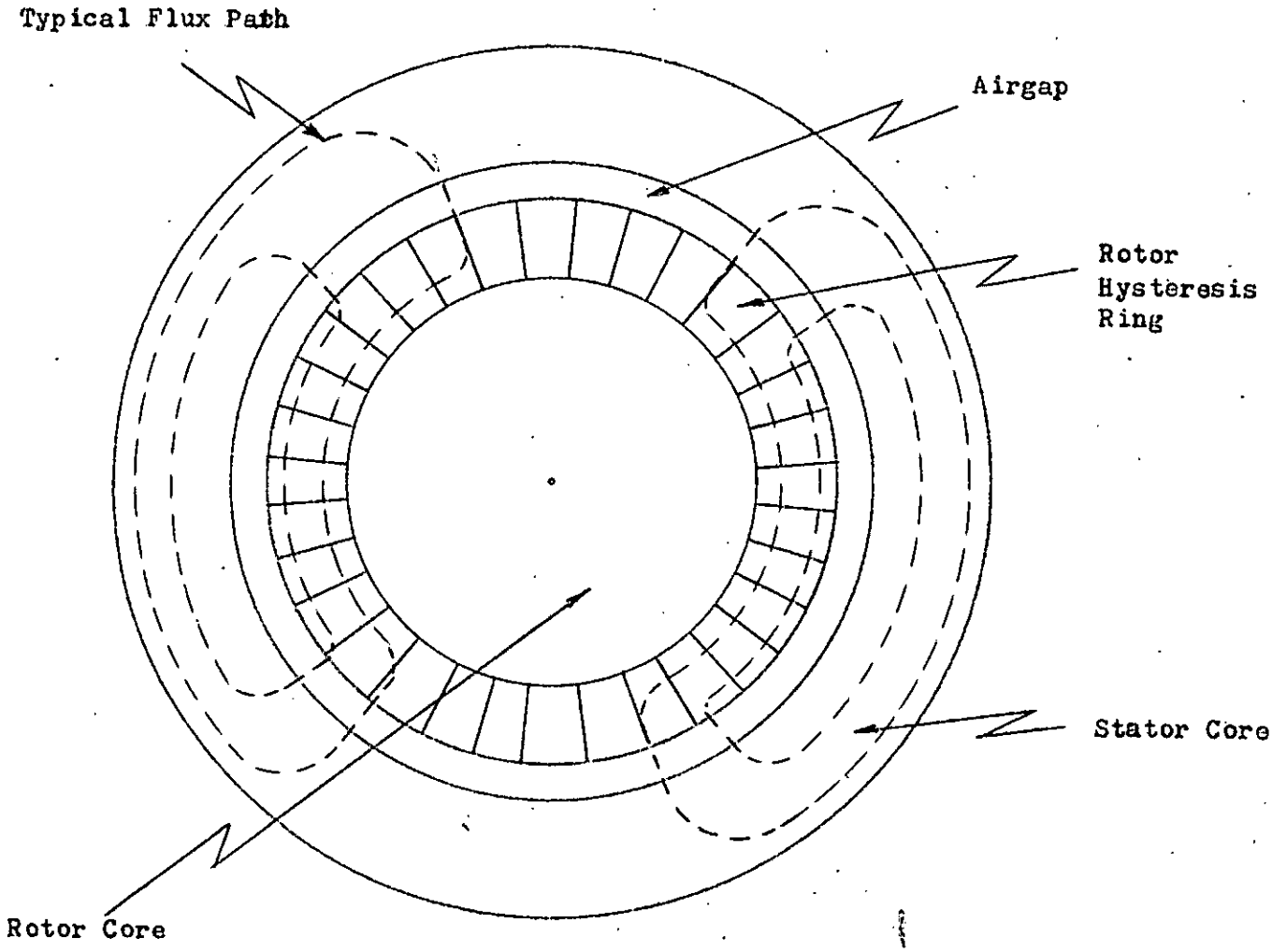

Fig.2b Typical Flux Path in Circumferential Flux Hysteresis Machine

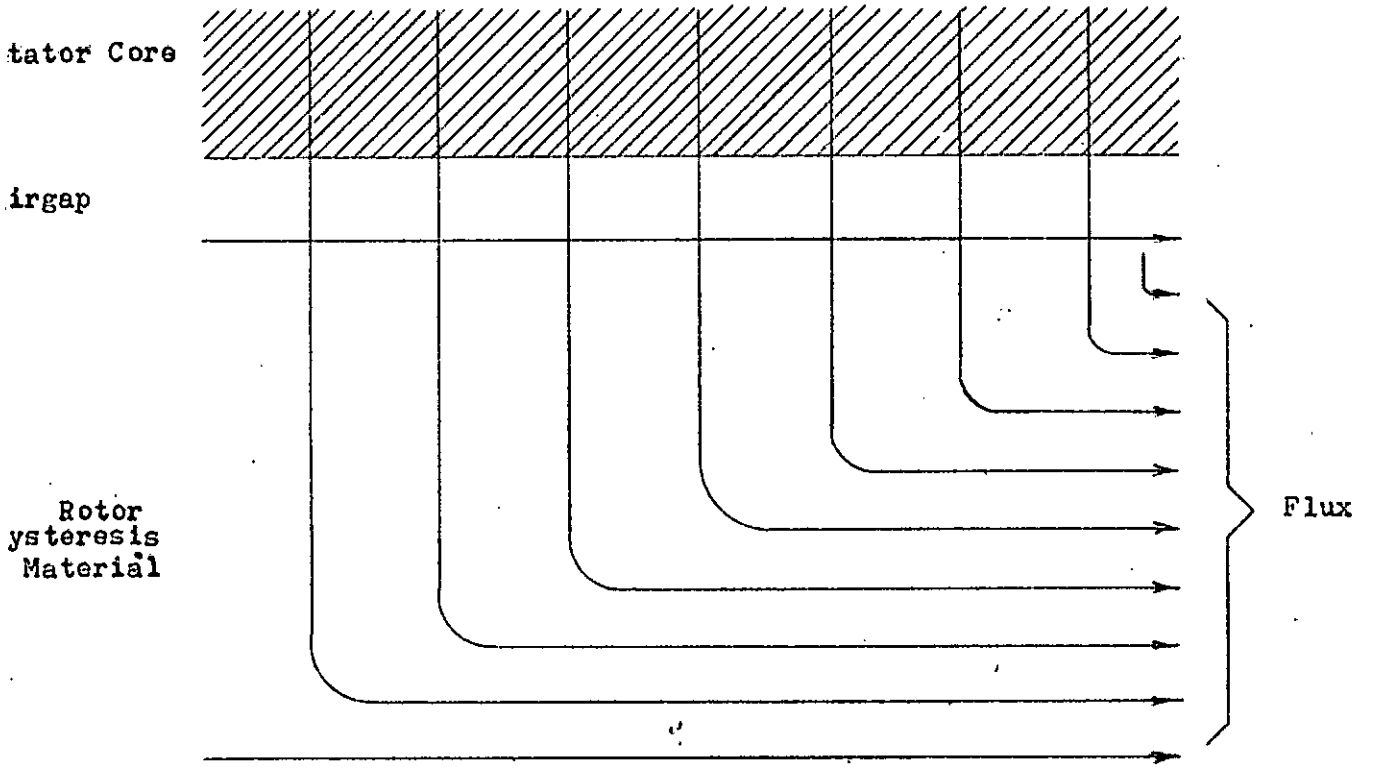

Fig. 3. Flux Patterns in Airgap and Hysteresis Ring in Circumferential Flux Hysteresis Machine.

In the case of an idealized radial flux hysteresis machine the following assumptions are made:

- Both the stator yoke and the rotor core has infinite permeability.
- The ring of hysteresis material of the rotor is considered to be divided into radial segments and no flux crosses the interfaces of the segments when passing through the magnetic ring.
- The total magnetic potential drop occurs across the series combination of the airgap and hysteresis ring only.

Thus, if a particular segment of the rotor including the corresponding airgap is considered, the magnetic potential across the series combenation is equal to the magnetic potential supplied by the stator current.

A more real and practial model is the circumferential - flux hysteresis machine. In this latter type, the rotor core is usually a non-magnetic one and is assumed to have infinite reluctance. Thus, the totoal potential drop occurs across the series combination of the airgap and the circumferential path covered by the flux along the hysteresis ring. The flux distribution in the airgap and in the hysteresis ring of an idealized circumferential flux hysteresis machine is shown in Fig.3.

In both the idealised hysteresis machine models, the space distribution of a stator winding is assumed to be ideally sinusoidal and the current entering the stator winding contains no time harmonies. This results a fundamental wave form of magnetomotive force rotating at synchronous speed in the airgap.

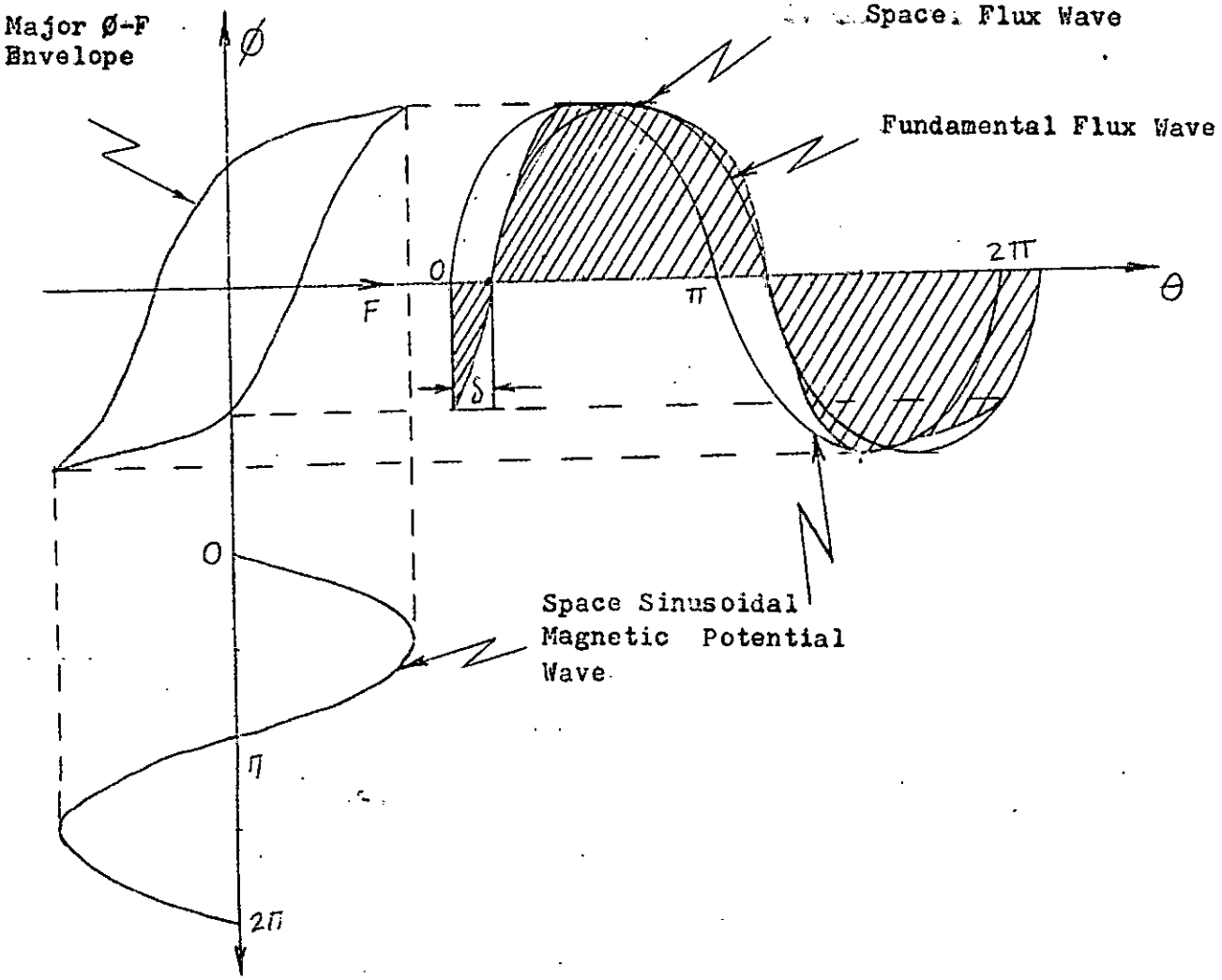

Fig.4. MMF And Flux Space Wave Relationship.

The effect of this magnetomotive force is to cause a non-sinusoidal airgap flux density wave envelope which also rotates at synchronous speed. This non-sinusoidal space flux wave may be expressed as Fourier Series.

The hysteresis machine develops its fundamental driving torque by virtue of the fact that this airgap flux density space wave lags the magnetomotive force space wave by an angle δ due to the non-linear relationship between B and H in the magnetic material. The relationship between the stator magnetomotive force space wave and the airgap flux space wave is shown in Fig.4.

The development of torque in a hysteresis machine occurs in two distinct and significant mechansims. The first and usually the predominant component is the hysteresis torque and the second one is the eddy current torque in the hysteresis ring. However, at synchronous speed the eddy current torque is zero and the motor is run by synchronous hysteresis torque.

At present this type of machine is widely used as a driving means of time measuring devices, recording equipments, gyros and in general where constant torque and quiet operation are needed. It may now also be used as a low lift pump for irrigation[8] purpose, as the hysteresis motors with integral hours power shaft torque are available[9].

2. PRINCIPLE OF OPERATION OF HYSTERESIS MACHINE.

The hysteresis motor can be regarded as a self starting synchronous motor. When the stator is excited by a balanced polyphase currents a sinusoidally varying MMF wave rśvolving at synchronous speed is established in the airgap. This MMF wave induces a nonsinusoidal flux density wave in the rotor hysteresis ring material. Due to the hysteresis effect of the rotor material the fundamental of the flux density wave lags behind the exciting MMF. Thus there exist an H-Wave and a B - wave in the rotor magnetic material separated in space by an angle which is the required condition for the production of torque.

Referring to Fig.5b the axis of the stator MMF and the axis of the rotor magnetization are not in phase. The axis of the rotor magentization lags behind that of the stator MMF by an angle . Referring back to Fig.5a if the stator and the rotor materials are of same nature like ordinary ferromagnetic material then the axis of the rotor magnetization is practically in line with stator MMF axis. And thus there is no appreciable phase shift between the stator MMF and the rotor flux density as in conventional rotating machines. But, however, in the case of hysteresis motor the hysteresis material of the rotor ring is made of 17% cobalt-nickel alley or specially heat treated low coercieve force alnico - v material.

These type of materials inherently exhibits a significant hysteresis effect. As the term hysteresis literarily means to fall back, therefore, the magnetization in the rotor ring has a tendency to lag behind the imposed reseolving MMF of the stator which has conventional ferro magnetic core. This angle of lag , as shown in Fig.5b is primarily due to the hysteresis characteristic of the rotor material. It is usually constant for a given material and is independent of stator excitation. The torque developed in the hysteresis motor is proportional to the sine of this angle . The expression for the torque of a hysteresis motor can be written as

$$T = k F \phi \sin \delta$$

Where F is stator MMF

is rotor flux,

and k is a constant.

For a given value of stator excitation, the stator MMF and rotor flux is usually constant and thus the above torque expression leads to a constant built in torque.

Further more, it may be noted that at starting i.e. with $S = 1$, the eddy current contributes the entire torque. At any speed other than Zero upto synchronous speed the torque in the hysteresis machine is due to both eddy current and hysteresis. At synchronous speed with $S = 0$, when the rotor is in synchronism with the stator MMF the Contribution of eddy current torque is zero and the motor is exclusively run by the hysteresis torque.

At synchronous speed since the rotor is under the influence of constant rotating MMF, the hysteresis material remain magnetized and develops as if d.c. magnetized poles like that of ordinary synchronous motors. This is why the rotor remains in synchronism so long as the stator excitation i.e. the airgap MMF field is maintained. This rotor magnetization which is analogous to the d.c. excitation of conventional synchronous motors can be conveniontly represented as a d.c. source. This is shown as E_p in the equivalent circuit models.

2. REVIEW OF LITERATURE:

The concept of the use of hysteresis energy in producing torque was first explored by steinmetz[1] towards the begining of the twentieth Century. Next Teare[2] in 1940 developed the theory of hysteresis motor torque based on the known field configurations of magnetic flux and magnetomotive force in the hysteresis material of the rotor and its dimensions. Then Roters[3] in 1947 used hysteresis lag angle and total loop energy in analysing the theory of the development of torque in hysteresis motor and also showed that parasitic hysteresis losses that are associated with the rotor caused by local ascillations could be greatly reduced using closed slots in the stator. This led to practical hysteresis motor in the fractional horse power range. However, as the operating characteristics of the motor have never been adequately explained and the improvement of the magnetic materials to have more energy per unit volume is limited, the commercial production of hysteresis motor is limited in the fractional hourse-power range. Hysteresis motors have the following advantages:-

- Simple rotor construction.
- Flat torque speed characteristics.
- Built in synchronizing driving torque.
- No starting problem as it can accellerate all the load that it can carry.

Because of the above mentioned merits of hysteresis motor it has potential for use as small synchronous motor in the advancing technology.

In recent years, Slemon and Copeland [4-5] analysed the synchronous operating characteristics of the hysteresis machine using idealised model for the hysteresis loop of its rotor material. But the output shaft torque could not be predicted, as it is difficult to predict the parasitic losses associated with the rotor materials which have an inherent non-linear behaviour.

Rahman [6 - 7] recently presented a complete analysis for predicting the parasitic losses in terms of machine geometry and magneto-electric characteristics of the hysteresis material. Once the parasitic loss phenomena are tackled higher rating hysteresis motor upto 4(four) horse power have been developed by Rahman[10] . All the above analysis are however limited to the case of synchronous mode of operation of the hysteresis motor. These analysis were approximate, as these are limited to the idealized case of synchronous hysteresis motor neglecting stator iron loss and saturation effects. The equivalent circuits developed so far did not truely represent the general circuit model of the motor.

Thus the scope of the present investigation is to develop a general analytical model for polyphase hysteresis motor at both synchronous and sub-synchronous speeds. Using parallogram approximations, general expressions for the terminal quantities are obtained. Steady - state equivalent circuit models are developed for both the synchronous and sub-synchronous mode of operation. The parasitic losses associated with the rotor hysteresis material, the stator iron losses and saturation effects are represented by suitable parameters in the general equivalent circuit model.

Chapter two contains the treatment of B - H loop which is lenearised using parallelogram model. It also contains the analysis of rotor parasitic losses, stator iron loss and stator saturation effects.

In chapter three equivalent circuit model for synchronous modes are derived. Basic equivalent circuit, general equivalent circuit and modified general equivalent circuit have also been developed.

Chapter four contains the derivation of equivalent circuits for sub-synchronous mode of operation. The expressions for equivalent hysteresis and eddy current resistances are obtained.

In Chapter five the discussions and conclusions are given.

CHAPTER II

1. TREATMENT OF B-H LOOP

One of the major problems in the development of the theory of hysteresis machine is the treatment of B-H Loop of the rotor hysteresis material which has a non-linear characteristic as shown in Fig.6. The analysis of the machine becomes prohibitive if one adheres strictly to the actual hysteresis loop. For the purpose of analysis, the B-H characteristic may be conveniently approximated by either (i) an elliptic or (ii) a parallelogram model which approximately represents the area contained in the actual hysteresis loop.

The hysteresis loop was replaced by inclined ellipse first by Teare[2] in his analysis of hysteresis motor. The elliptical representation was further extended by Roters [3] and Miyairi[12] for the fractional hourse-power hysteresis machine. Later Copeland and Slemon[4-5] introduced the parallelogram modelling of the B-H loop to predict fundamental developed torque in terms of machine dimensions and hysteresis material characteristics.

It is evident from Fig.7 that the area contained in the elliptical model of the loop does not fully represent the actual area of the loop. The major discrepancy is due to the poor approximation at the tips of the loop. However, in parallelogram modelling the area of the loop is more accurately approximated.

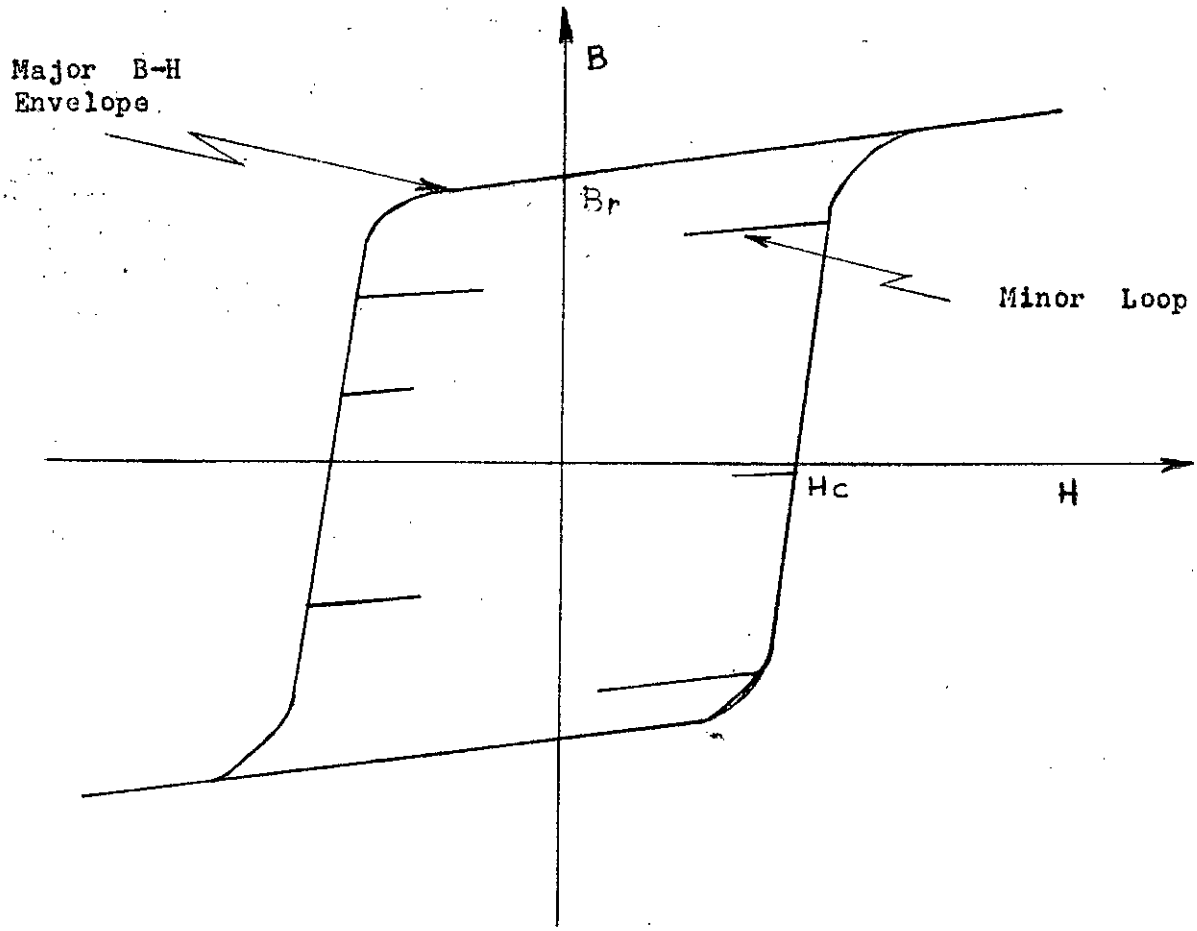

Fig.6. B-H Loop. Non-linear Characteristic of Hysteresis Material.

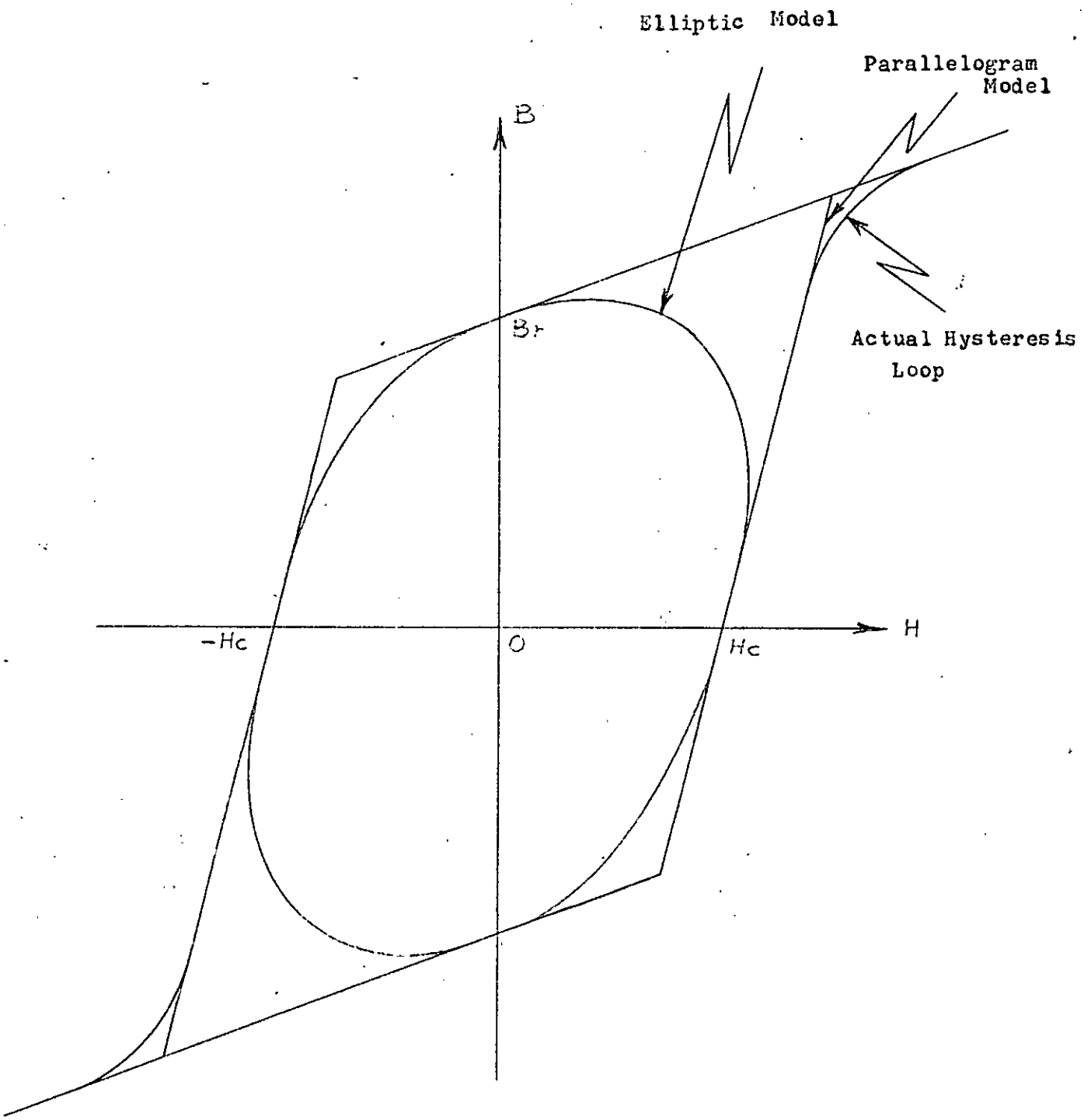

Fig.7. Modelling of Hysteresis Loop by Parallelogram and Ellipse.

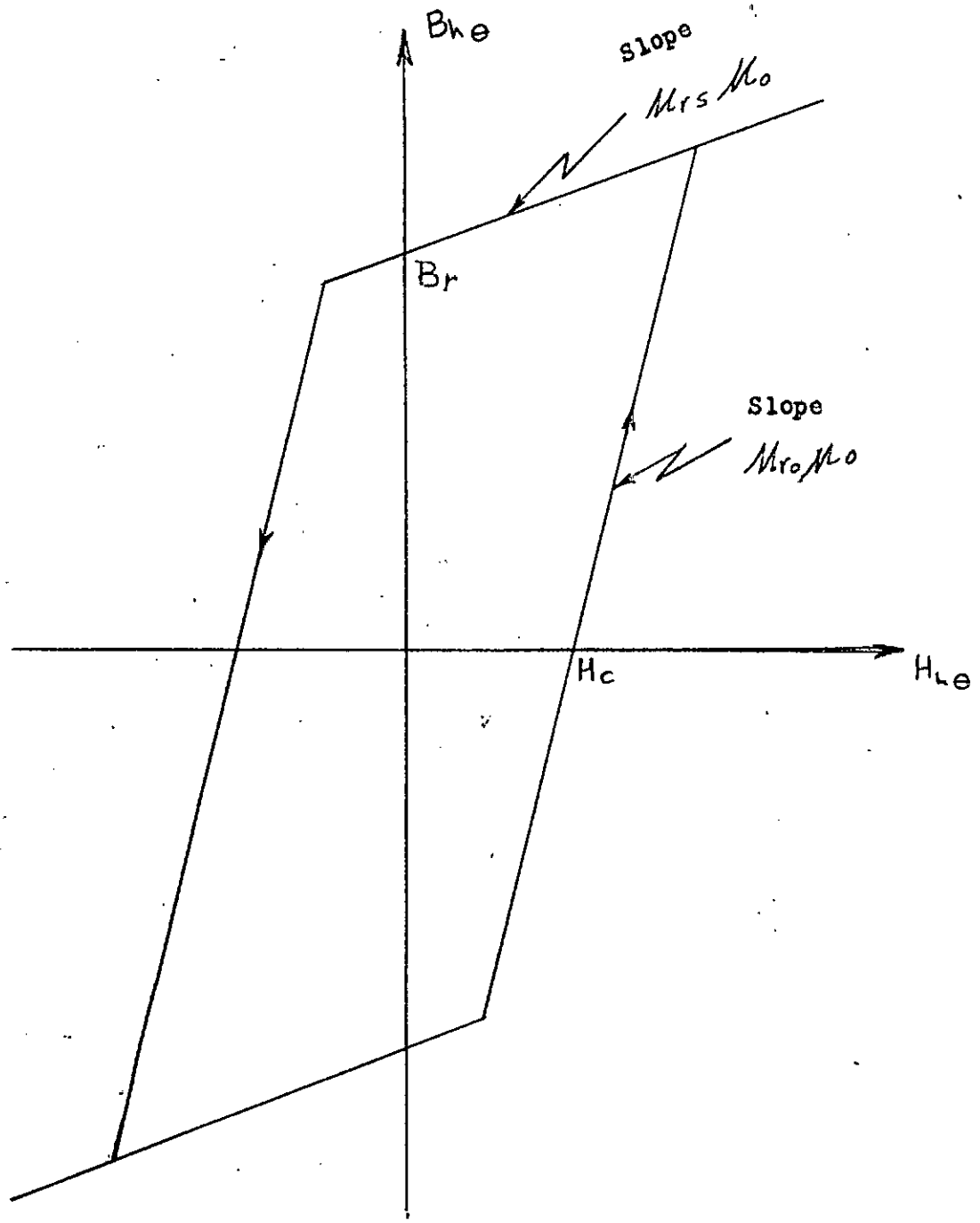

Fig.8. Idealized Magnetization Characteristics for Hysteresis Material.

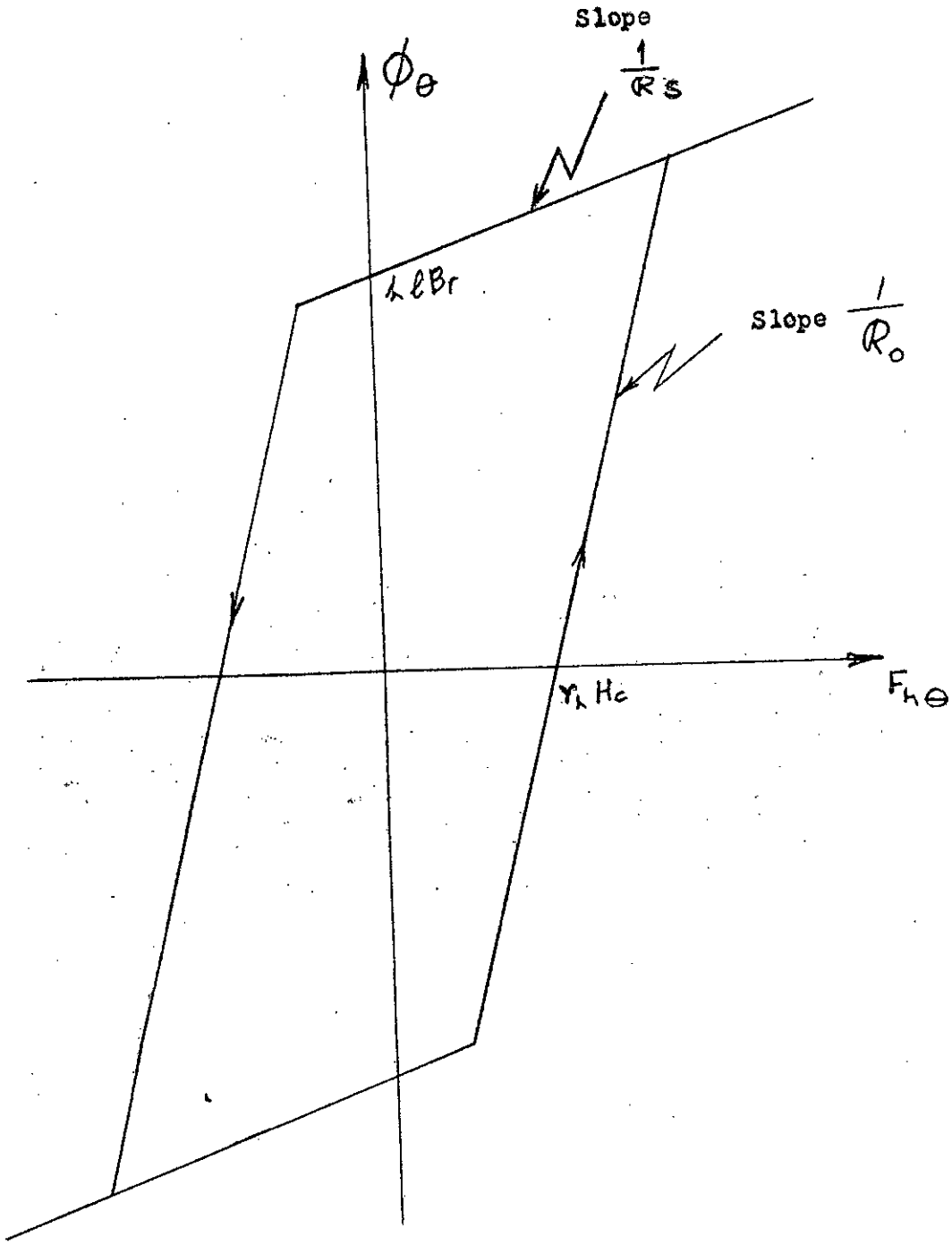

Fig.9. Flux Versus Magnetic Potential in Hysteresis Material.
(per unit angle)

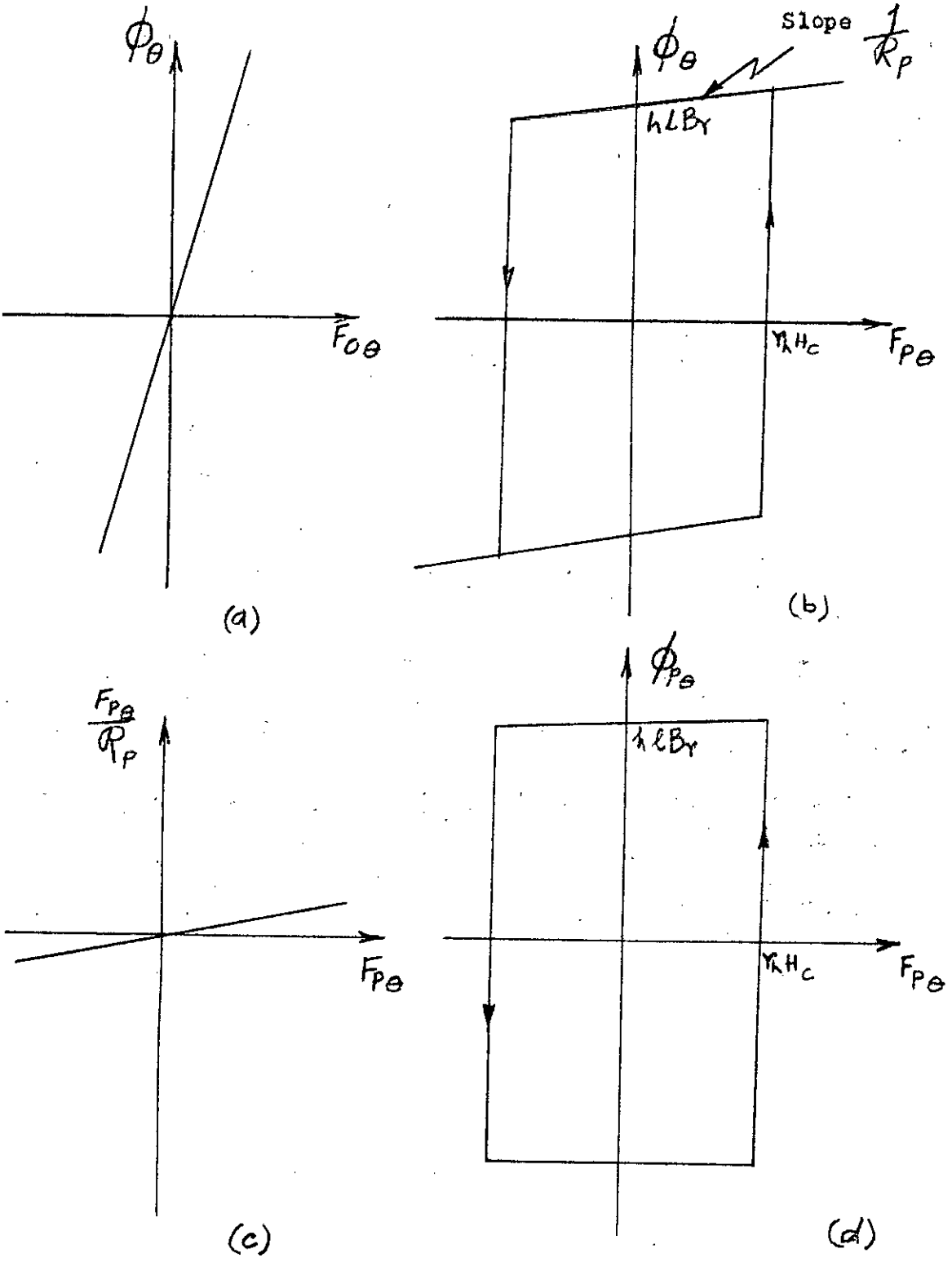

Fig.10. Steps in Producing a Simplified Model of Fig.9.

(a) Reluctance Per Unit Angle R_o.

(b) Original Loop of Fig.9 with Series R_o Subtracted.

(c) Reluctance Per Unit Angle R_p.

(d) Loop of Fig.10(b) with Parallel R_p Subtracted.

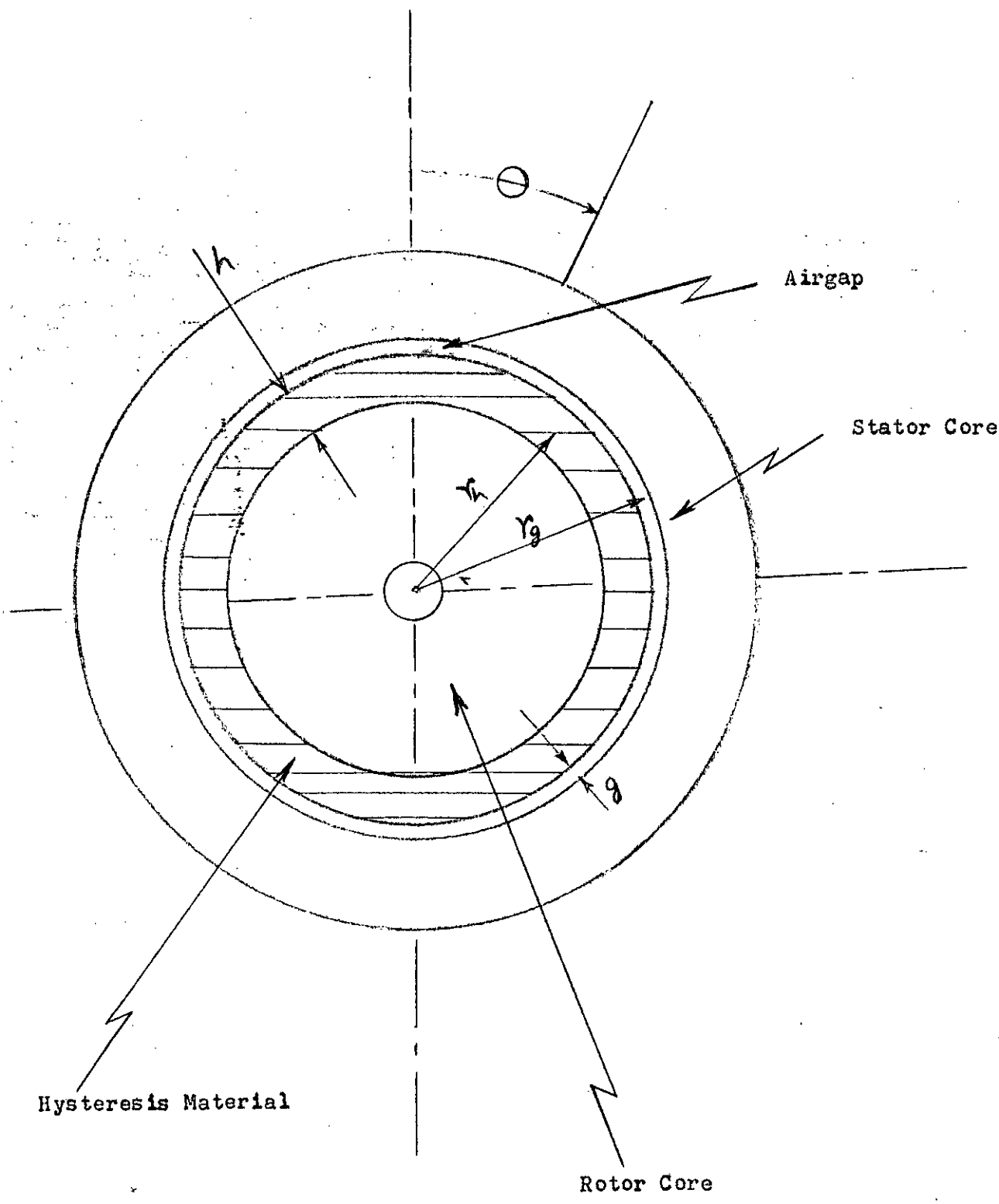

Fig.11. Cross -Section of Hysteresis Machine Showing Dimensions.

The areas of the actual loop left outside the edge of the parallelogram at two ends are accounted for by including almost equal areas at the other two ends. Thus the parallelogram model may be a better approximation than the elliptical model.

To analyse the theory of hysteresis machine using parallelogram model it is assumed that the B-H loop of the hysteresis material is a parallelogram of constant width equal to twice the co-ercive force H_c and height equal to twice the residual flux density B_r , i.e.

$$\text{Width} = 2 H_c \tag{1}$$

$$\text{and Height} = 2 B_r \tag{2}$$

and the slope of the vertical sides and the outer boundary of the loop are $\mu_{ro}\ \mu_o$ and $\mu_{rs}\ \mu_o$ respectively where μ_{ro} is defined as the un-saturated relative permeability, μ_{rs} , the saturated relative permeability, and μ_o , as the permeability of free space. This shown in Fig.8.

This B-H loop of Fig.8 may be transformed to ϕ - F envelop as shown in Fig.9. The conversion factors for a circumferential flux hysteresis machines are :

$$\phi_\theta = B_{h\theta}\ hl \qquad \text{Webers} \tag{3}$$

$$F_{h\theta} = H_{h\theta}\ r_h \qquad \text{amperes} \tag{4}$$

where ϕ_θ = flux at angle θ ,

$F_{h\theta}$ = magnetic potential drop across the hysteresis material,

B_{he} = flux density in hysteresis material at angle θ ,

$B_{h\theta}$ = magnetic field intensity in the hysteresis material at angle θ,

h = thickness of hysteresis ring,

l = axial length of the rotor,

and r_h = radius to centre of the hysteresis ring.

The dimensions are shown in Fig.11.

Any flux excursion on the ϕ - F loop is governed by straight - line relation of the form $y = mx + c$, where $1/\mathcal{R}_o$ is the slope if the state point is on the left or right hand sides of the loop, and $1/\mathcal{R}_s$ if the state point is within the outer boundaries of the loop. These incremental reluctances per unit angle are given by the expressions:

$$\mathcal{R}_o = \frac{r_h}{\mu_{ro}\,\mu_o\,hl} \quad \text{amperes/weber-radian} \qquad (5)$$

$$\mathcal{R}_s = \frac{r_h}{\mu_{rs}\,\mu_o\,hl} \quad \text{amperes/weber-radian} \qquad (6)$$

This ϕ - F Parallelogram model of Fig.9 may be simplified as follows:

The unsaturated linear reluctance $\mathcal{R}_o$ per unit angle may be conceived of in series with the vertically sided ϕ - F characteristic as shown in Fig.10(a) and (b). This linear reluctance $\mathcal{R}_o$ of Fig.10(a) has an effect which is equivalent to an extension of the airgap resulting new loops of vertical sides i.e. zero reluctance. Because of the subtraction of $1/\mathcal{R}_o$ everywhere from the slope of the loop, any flux excursion

within the outer bounderies of the new loops will occur with a slope $1/\mathcal{R}_p$ where

$$\mathcal{R}_p = \mathcal{R}_s - \mathcal{R}_o \tag{7}$$

Substituting values of $\mathcal{R}_s$ and $\mathcal{R}_o$ from equation (5) and (6), we get

$$\mathcal{R}_p = \frac{r_h}{\mu_o \; hl}\left(\frac{1}{\mu_{rs}} - \frac{1}{\mu_{ro}}\right)$$

$$= \frac{r_h}{\mu_o \; hl}\left(\frac{\mu_{ro} - \mu_{rs}}{\mu_{ro} \; \mu_{rs}}\right)$$

$$= \frac{r_h}{\mu_p \; \mu_o \; hl} \qquad \text{ampere/weber - radian} \tag{8}$$

where μ_p is defined as the equivalent permeability

and $$\mu_p = \frac{\mu_{ro} \; \mu_{rs}}{\mu_{ro} - \mu_{rs}} \tag{9}$$

The non-linear characteristic of Fig.10(b) can be further simplified by representing it as a linear reluctance per unit angle R_p in parallel with a ractangular loop non-linear element as shown in Fig.10(c) and (d).

2. PARASITIC LOSSES

The parasitic losses [6] associated with the hysteresis ring act as a major detriment to the efficiancy and performance of the hysteresis machine. The parasitic losses may be sub-divided into two components, namely the MMF-Parasitic Loss and the Flux-Parasitic Loss, on the basis of their distinct sources of origin.

In a practical machine sinusoidal distribution of winding cannot be realised in practice because of the finite number of turns and the distribution of windings in a limited number of slots. Due to this non-sinusoidal distribution ofwinding the revolving mmf-space wave contains space harmonies which are the functions of pitch and distribution factors of the stator winding. In a hysteresis machine these space harmonics causes the rotor material to experience minor hysteresis loops. Typical minor loops [13] superimposed on the major B-H loop is shown in Fig.6. The loss associated with these minor loops is defined as the MMF-Parasitic Loss.

Minor loops are also developed due to the presence of tooth ripple in the airgap flux density space wave. The rotor material experiences such tooth ripple when it passes from the short airgap under the tooth face to the relatively long airgap under the slot opening. The minor loops are superimposed on the major B-H loop at the tooth ripple frequencies. The loss associated with these minor loops is denoted as the Flux-Parasitic Loss.

The losses associated with the minor loops caused by both the tooth ripple present in the airgap flux density space wave and space harmonics present in the stator mmf - space wave consist of hysteresis and eddy-current effects of the minor loops. But the eddy current effect is predominent [13] for materials commonly used in

hysteresis machine. The hysteresis loss of the minor loops with most metallic permanent magnet materials is less than 4 percent [7] of the eddy-current loss. Thus the hysteresis effect of minor loops may be ignored and a general expression for the parasitic losses due to eddy-current effect only may be developed.

Rahman, Copeland and Slemon [6] derived a general expression for the parasitic losses due to eddy-current effect only(neglecting hysteresis effect) in terms of machine dimensions, airgap field,stator current and rotor hysteresis material characteristic for the synchronous mode of operation of the hysteresis machine using a current sheet model and assuming linear minor loop permeability. In their analysis space harmonics of order n were assumed in the mmf - space wave. For the nth harmonic space wave the wave length is λ / n where λ is the wave length of the fundamental component and the angular frequency of the induced rotor eddy-current at synchronous speed becomes

$$w = 2 \pi f_n \qquad (10)$$

where f_n is the frequency of the nth harmonic. This is the frequency at which the minor loop excursions in the rotor material due to mmf - harmonics happen and is given by the expression

$$f_n = n\left(1 \pm \frac{1}{n}\right) f_1 = (n \pm 1) f_1 \qquad (11)$$

where f_1 is the frequency of the fundamental component. The expression for the mmf - parasitic loss per unit surface area for the nth harmonic

of an m - phase hysteresis machine having rms stator phase current I_s in amperes is given[6] by

$$P_{mn} = K_{mn} I_s^2 \tag{12}$$

where $$K_{mn} = \frac{(1 \pm 1/n) f1 \mu_r \mu_o \beta_\eta m^2 z^2}{[(\mu_r + \gamma_n)^2 + \beta n^2]\lambda}$$

$$\left(\frac{\sin(n\pi s/\lambda)}{n\pi s/\lambda}\right)^2 K_{dn}^2 K_{pn}^2 = 4n\pi\delta/\lambda \tag{13}$$

where $$\gamma = \left[1/2(1 + (1 + \chi^4)1/2\right] 1/2 \tag{14}$$

$$\beta = \left[1/2(-1 + (1 + \chi^4)\ 1/2\right] 1/2 \tag{15}$$

and $$\chi = \frac{1}{\sqrt{2}\pi} \cdot \frac{\lambda}{\sigma} \tag{16}$$

σ is the skin depth,

and $$\sigma = \left(\frac{2\rho}{w \mu_r \mu_o}\right)^{1/2} \tag{17}$$

ρ is the resistivity of the rotor hysteresis material,

z is the number of conductors per phase per pole,

δ s is the width of the stator slot and

K_{pn} and K_{dn} are the harmonic pitch and distribution factors respectively.

For an m-phase hysteresis machine operating under balanced conditions, the harmonic terms which exist are those for which $(n \pm 1)/m$ is an integer. The total mmf - parasitic loss per unit surface area for a three phase machine may be expressed as

$$P_m = K_m I_s^2 \tag{18}$$

where $K_m = \sum_n K_{mn}$, $n = 5,7,11,13 \ldots\ldots$ (19)

which shows that the mmf - parasitic loss is directly proportional to the square of the rms stator current.

Similarly, from the eddy current caused by the tooth ripple in the airgap field the flux - parasitic loss may be expressed as [6]

$$P_f = \frac{f_t \lambda \beta}{2 \mu_r \mu_o} \hat{B}^2 \tag{20}$$

where f_t is the basic tooth ripple frequency and is given by

$$f_t = 2 s_1 f_1 \tag{21}$$

S_1 being the number of stator slots per pole

and $\lambda = p$ i.e. the wave length of the fundamental induced rotor current due to the tooth ripple flux is equal to the stator slot pitch p.

Now, due to the effect of the variable gap reluctance tooth ripple harmonics will be present in the airgap flux density space wave. The peak airgap flux density(for the ith component) $\hat{B}_i$ may be related with the peak value $\bar{B}$ of the mean flux density in the airgap neglecting the ripple component, as

$$\hat{B}_i = a_i \eta_i \bar{B} \tag{22}$$

where a_i and η_i are the factors and

$$a_i = \hat{B}_i / \bar{B} \text{ , neglecting eddy current effect,} \tag{23}$$

and η_i is called the reduction factor i.e. the factor by which the harmonic airgap field is reduced when the eddy current effect is included and is given as

$$\eta_i = \frac{\mu_r + 1}{\left[(\mu_r + \gamma_i)^2 + \beta_i^2\right]^{1/2}} \tag{24}$$

Thus substituting eqns. 21 and 22 in eqn.20, we get the total flux - parasitic loss as

$$P_f \neq \frac{S_1 f_1^p \beta_i a_i^2 \eta_i^2}{\mu_r \mu_o} \left(\frac{\ell}{B}\right)^2 \tag{25}$$

$$= K_f \bar{B}^2 \tag{26}$$

where $$K = \sum_{i} \frac{S_1 f_1^p \beta_i a_i^2 \eta_i^2}{\mu_r \mu_o}, \quad i = 1,2,3 \ldots\ldots \qquad (27)$$

Now, the airgap voltage

$$E_g = 4.44 f N_s \bar{B}_g k_d k_p$$

$$= K \bar{B}_g \qquad (28)$$

where $$K = 4.44 f N_s k_d k_p \qquad (29)$$

Therefore,

$$P_f = K_f \cdot E_g^2 / K^2 , \quad \bar{B} = \bar{B}_g$$

$$= K'_f E_g^2 \qquad (30)$$

where $$k'_f = K_f / K^2 \qquad (31)$$

which shows that the flux - parasitic loss is directly proportional to the square of airgap flux - density and hence to the square of airgap voltage.

3. STATOR IRON LOSS

Accurate treatement of stator iron loss is really a difficult job. Trickey[14] in his analysis developed some convenient empirical formula for the iron loss of small motors. He showed that for small polyphase hysteresis motors having rating upto few integral hourse-powers and operated at synchronous speed, the fundamental frequency iron loss is, usually, composed of the losses in the yoke and the teeth. This stator iron loss may be represented by an equivolent resistance R_i which is dependent upon the total flux.

4. SATURATION IN STATOR CORE.

In a paractical machine the sinusoidally distributed magnetomotive force is absorbed in producing a non-sinusoidal flux density in the airgap, the stator teeth, the stator yoke and the rotor hysteresis ring. Assuming temporarily that only tooth saturation is significant and that leakage fluxes are negligible, the magnetic field intansity around the path in the airgap, the stator tooth and the rotor ring may be found for a given values of airgap flux density. The summation of field intensity around the path gives the total magnetomotive force corresponding to the flux density. For the sinusoidally distributed magnetomotive force the corresponding flux density is the flat-topped distribution as shown in Fig.4. Only the fundamental space component of this flux density wave links with the sinusoidally distributed winding. This fundamental component is given by

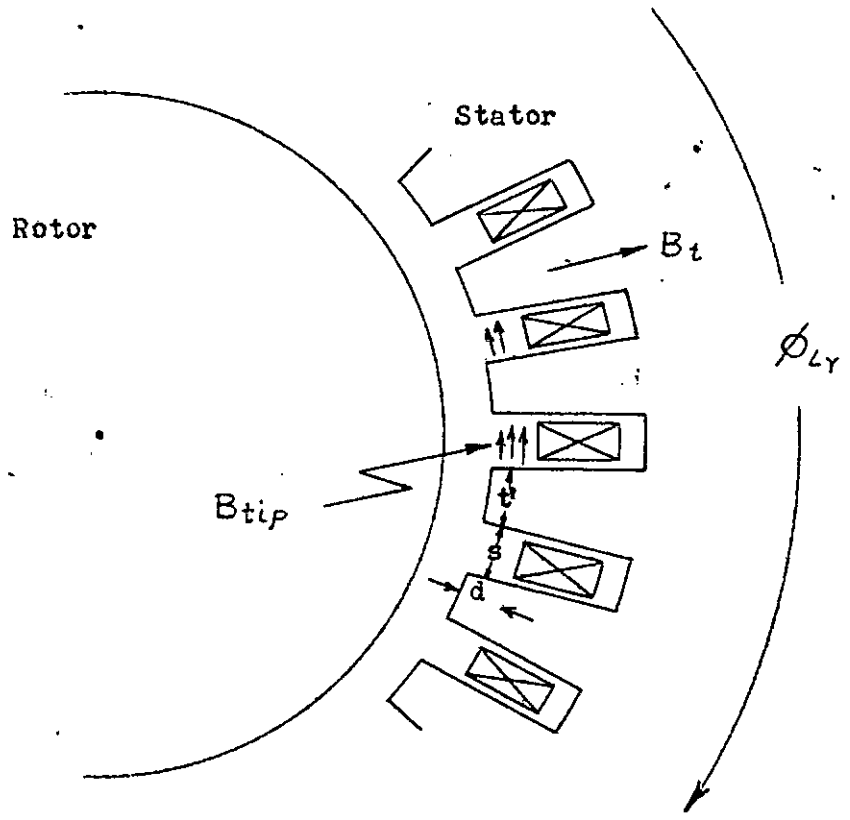

Fig.12. Stator Slot - Tooth Dimensions.

$$B_1 = \bar{B}_1 \cos\left(\omega t + \alpha_m + \frac{\pi}{2} - \frac{P\theta}{2}\right) \qquad (32)$$

Let us now examine the relation between the stator slot leakage flux and the airgap flux. The current per unit angle in the stator slot is

$$j_\theta = \frac{m N_s \hat{I}_s}{2\pi} \cdot \frac{2}{P} \cos\left(\omega t + \alpha - \frac{P\theta}{2}\right) \text{ amperes/Radian} \qquad (33)$$

Due to this stator current density a circumferential tip-to-tip leakage flux density will be developed which is given by

$$B_{tip} = \mu_o \frac{j_\theta}{g_e} \qquad (34)$$

where g_e is the effective circumferential airgap per unit angle and is given by

$$g_e = r \cdot \frac{s}{t' + s} \qquad (35)$$

using the dimensions of Fig.12 with machine radius r. The tip-to-tip circumferential flux is thus

$$\phi_{tip} = B_{tip} \cdot l \cdot d$$

$$= \mu_o m \frac{(t' + s)}{rs} \cdot l \cdot d \cdot \frac{N_s \bar{I}_s}{2} \cdot \frac{2}{P} \cos \left(wt + \alpha - \frac{P\theta}{2} \right) \text{ weber} \qquad (36)$$

where l is the machine length and d is the effective radial depth of the slot leakage flux path as shown in Fig.12. This tip-to-tip leakage flux can saturate the tooth tips due to stator current along. Its maximum value occurs at $\frac{P\theta}{2} = wt + \alpha$. Its interaction with the airgap flux can be appreciated by considering a situation in which the stator current is entirely magnetizing i.e. $\alpha = \alpha_m$, as with a zero - power - factor leading load. Comparison of eqns.32 and 36 shows that the tip-to-tip leakage flux is in space quadrature with the airgap flux for this condition allowing the saturation due to the two flux components to be considered independantly. Interaction of the two flux component may be important for near unity power factor loads for which $\alpha \cong \alpha_m + \frac{\pi}{2}$. For this condition the two components are in space phase.

Again from this tip-to-tip circumferential leakage flux the radially directed leakage flux in the stator tooth may be derived as

$$B_t = \frac{1}{lr} \cdot \frac{d\phi_{tip}}{d\theta}$$

$$= \mu_o m \cdot \frac{t' + s}{r^2 sl} \cdot \frac{N_s \bar{I}_s}{2} \cdot \frac{2}{P} \cos \left(wt + \alpha + \frac{\pi}{2} - \frac{P\theta}{2} \right) \qquad (37)$$

where B_t is the average flux density over tooth and slot. Comparison of eqn.37 with eqn. 32 shows that this flux density is in space phase with the airgap flux density when $\alpha = \alpha_m$ i.e. for zero-power factor load conditions. The two components of tooth flux are also colinear and may be added directly to obtain the total tooth flux. For other values of stator current phase angle, the components space waves may be added vectorially to obtain the total tooth flux.

Thus we see that saturation in tooth body is a function of the total radially directed tooth flux which is a result of the vectorial sum of the sinusoidally distributed airgap and slot leakage flux components.

There are two more components of leakage flux. These are the tooth - top leakage and the zig-zag leakage components. Both of them are also caused by the stator current density. Therefore, the contribution of the two components to the tooth flux may also be considered with the radially directed flux in the stator tooth.

Now the flux in the yoke corresponding to the fundamental space component of the airgap flux at an angle θ is given by

$$\begin{aligned} \phi_{my} &= \int lr \quad B_1 \quad d\theta \\ &= - lr \quad \hat{B}_1 \quad \cos \left(wt + \alpha_m + \frac{P\theta}{2} \right) \text{ weber} \end{aligned} \tag{38}$$

And the component of the stator leakage flux ϕ_{Ly} in the yoke as seen from Fig.(12) is equal in magnetude and opposite in direction to the circumferential tip-to-tip leakage flux. Thus

$$\phi_{Ly} = -B_{tip}\, ld \cos\left(wt + \alpha - \frac{P\theta}{2} \right) \qquad (39)$$

Again the leakage and mutual flux components of the flux are colinear and in space phase when $\alpha = \alpha_m$. The ratio of the two components is the same as in the radial tooth flux.

The contribution of the space harmonics in the airgap flux to the yoke saturation is normally expected to be negligible. The contribution due to the largest harmonic does not usually exceed 3% of that of the fundamental.

CHAPTER III

1. DERIVATION OF EQUIVALENT CIRCUIT MODELS FOR IDEALISED HYSTERESIS MACHINE-Synchronous Mode.

Fig.11 shows the cross-section and dimensions of a polyphase hysteresis machine. The stator is assumed to have a sinusoidally distributed polyphase winding having N_s turns per phase and excited by a balanced set of polyphase currents. The current in phase a is

$$i_a = \bar{I}_s \cos (wt + \alpha_m) \qquad (40)$$

where m is the phase angle for zero-power factor load condition.

The rotor hysteresis ring is assumed to be homogeneous and its B-H characteristic is represented by a parallelogram as shown in Fig.8. The path of the magnetic flux is radial in the airgap and circumferential in the hysteresis material as shown in Fig.4. The magnetic flux distribution inside the ring is assumed uniform and there is no flux penetration into the rotor non-magnetic sleeve.

Considering a P-pole, m-phase machine the number of conductors per phase is

$$z = \frac{N_s}{\frac{P}{2}} \cdot \cos \frac{P\theta}{2} \quad \text{conductor/radian} \qquad (41)$$

and the total magnetic potential at angle θ is

$$F_\theta = \frac{m \cdot N_s \bar{I}_s}{2} \left(\frac{2}{P}\right) \cos \left(wt + \alpha_m + \frac{\pi}{2} - \frac{P\theta}{2}\right) \text{amperes} \qquad (42)$$

which describes a revolving magnetic field.

This total magnetic potential is obsorbed in producing a flux density in the airgap and the hysteresis ring in an idealised machine, that is

$$F_\theta = F_{g\theta} + F_{h\theta} \quad \text{amperes} \tag{43}$$

A magnetic flux ϕ_θ per unit angle of periphery will be established by the magnetic potential F_θ and this flux will be continuous through the airgap and the hysteresis material. The magnetic potential $F_{g\theta}$ across the airgap and the flux ϕ_θ per unit angle are related by the airgap reluctance per unit angle,

$$\mathcal{R}_{g\theta} = \frac{\delta_\theta}{\mu_o r_g l} \quad \text{ampere/weber-radiam} \tag{44}$$

The mmf drop in the air gap is then

$$F_{g\theta} = \mathcal{R}_{g\theta} \phi_\theta = \frac{\delta_\theta}{\mu_o r_g l} \phi_\theta \quad \text{amperes} \tag{45}$$

In the hysteresis material the magnetic flux per unit angle ϕ_θ is related to the magnetic potential $F_{h\theta}$ by the idealized magnetization characteristic as shown in Fig.9.

Simplifying this ϕ - F envelop of Fig.9 to Fig.10(d) we get,

$$F_{h\theta} = F_{o\theta} + F_{p\theta} \quad \text{ampere} \tag{46}$$

$$\text{and} \quad \phi_\theta = \phi_{p\theta} + F_{p\theta} / \mathcal{R}_p \quad \text{weber} \tag{47}$$

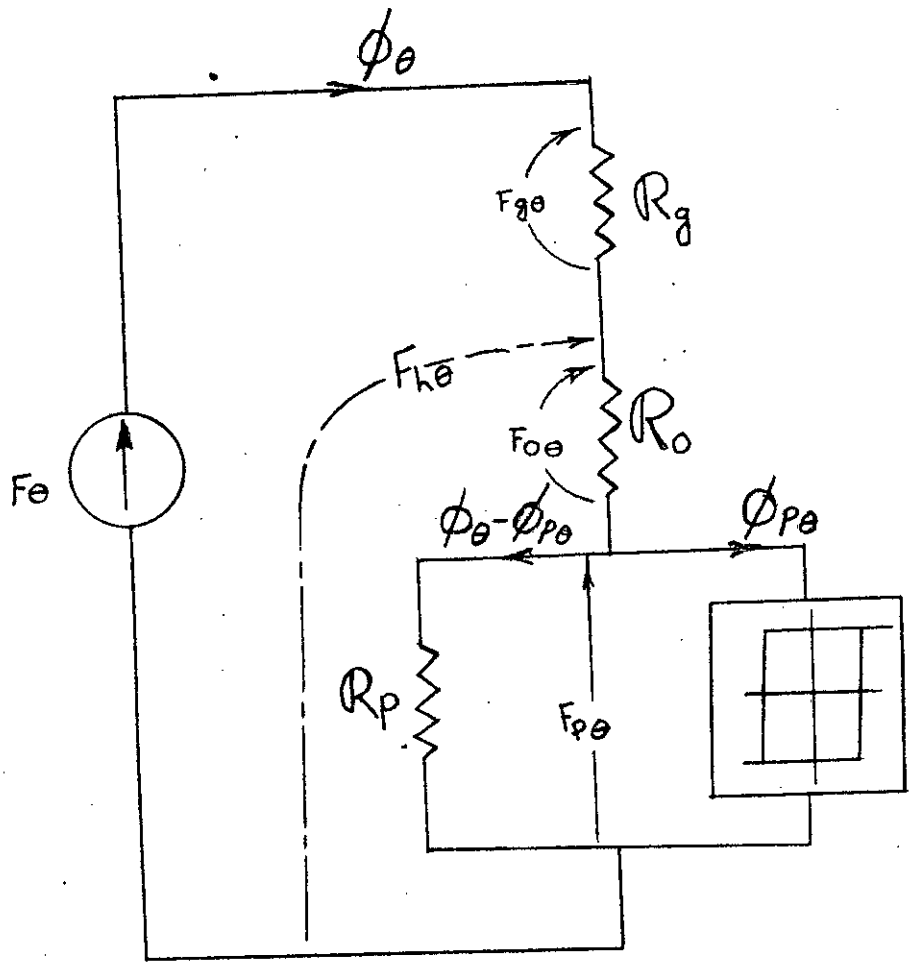

Fig.13. Approximate Magnetic Equivalent Circuit.

The magnetic equivalent circuit of the hysteresis motor is shown in Fig.13. The matrix statement for this circuit problem is

$$\begin{bmatrix} F_\theta \\ 0 \end{bmatrix} = \begin{bmatrix} \mathcal{R}_g + \mathcal{R}_o + \mathcal{R}_p & -\mathcal{R}_p \\ -\mathcal{R}_p & \mathcal{R}_p + \boxplus \end{bmatrix} \begin{bmatrix} \phi_\theta \\ \phi_{p\theta} \end{bmatrix} \tag{48}$$

The corresponding dual electric equivalent circuit of Fig.13 is shown in Fig.14 and the matrix equation describing the dual electric equivalent circuit is

$$\begin{bmatrix} I_s \\ 0 \end{bmatrix} = \begin{bmatrix} \frac{1}{jX_g} + \frac{1}{jX_p} + \frac{1}{jX_p} & -\frac{1}{jX_p} \\ -\frac{1}{jX_p} & \frac{1}{jX_p} + \boxplus \end{bmatrix} \begin{bmatrix} E_g \\ E_p \end{bmatrix} \tag{49}$$

where

$$jX_g = jw \frac{m\pi}{8} \left(\frac{2}{p}\right)^2 \frac{N_s^2}{\mathcal{R}_g}$$

$$= jw\ L_g \tag{50}$$

$$jX_o = jw \frac{m\pi}{8} \left(\frac{2}{p}\right)^2 \frac{N_s^2}{\mathcal{R}_o}$$

$$= jw\ L_o \tag{51}$$

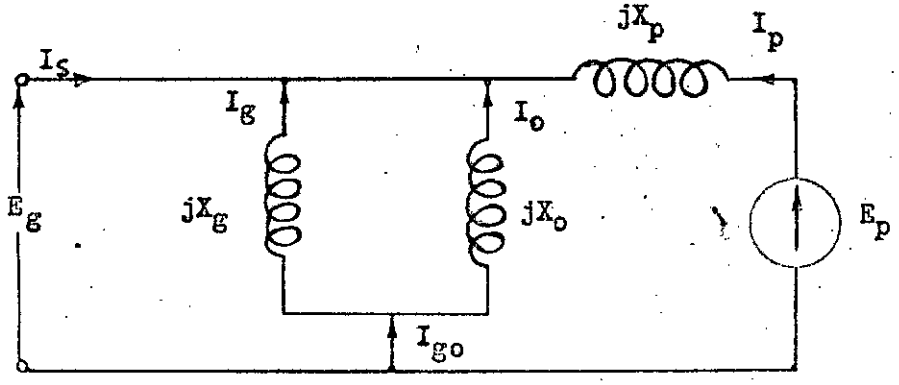

Fig.14. Electric Equivalent Circuit for Idealized Hysteresis Machine.

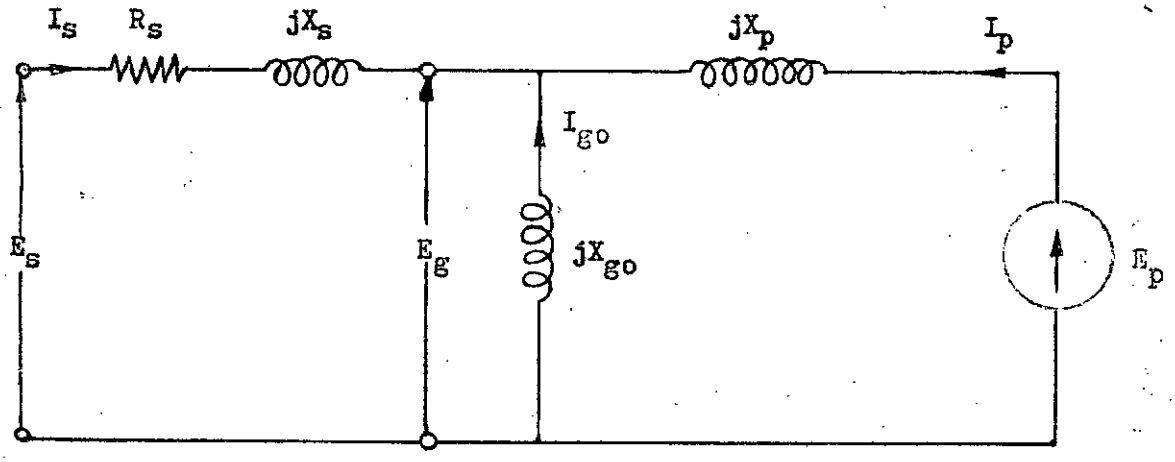

Fig.15. Modified Electric Equivalent Circuit for Idealized Hysteresis Machine Including Stator Impedances.

$$jX_p = jw\frac{m\pi}{8}\left(\frac{2}{P}\right)^2 \frac{N_s^2}{\mathcal{R}_p}$$

$$= jw\,L_p \qquad (52)$$

From eqn. 50, 51 and 52 the inductances L_g, L_o and L_p are

$$L_g = \frac{m\pi}{8}\left(\frac{2}{P}\right)^2 \frac{N_s^2}{\mathcal{R}_g}$$

$$= \frac{m\pi}{8}\left(\frac{2}{P}\right)^2 N_s^2 \frac{\mu_o r_g l}{g_\theta} \quad \text{henry} \qquad (53)$$

$$L_o = \frac{m\pi}{8}\left(\frac{2}{P}\right)^2 \frac{N_s^2}{\mathcal{R}_o}$$

$$= \frac{m\pi}{8}\left(\frac{2}{P}\right)^2 N_s^2 \frac{\mu_{ro}\mu_o hl}{r_h} \quad \text{henry} \qquad (54)$$

and $$L_p = \frac{m\pi}{8}\left(\frac{2}{P}\right)^2 \frac{N_s^2}{\mathcal{R}_p}$$

$$= \frac{m\pi}{8}\left(\frac{2}{P}\right)^2 N_s^2 \frac{\mu_o hl}{r_h} \cdot \frac{\mu_{ro}\mu_{rs}}{\mu_{ro}-\mu_{rs}} \quad \text{henry} \qquad (55)$$

The equivelent circuit of Fig.14 may be shown in ~~Fig.(15)~~ a more familiar form as shown in Fig.(15) including the stator impedances. The phasor equations may be expressed in the matrix form as

$$\begin{bmatrix} E_s \\ E_p \end{bmatrix} = \begin{bmatrix} R_s + j(X_s + X_{go}) & jX_{go} \\ jX_{go} & j(X_{go} + X_p) \end{bmatrix} \begin{bmatrix} I_s \\ I_p \end{bmatrix} \qquad (56)$$

where $$jX_{go} = j\frac{X_g X_o}{X_g + X_o} \qquad (57)$$

Using the expressions of eqns.(50) and (51) we get

$$jX_{go} = jw\left(\frac{L_g L_o}{L_g + L_o}\right) \qquad (58)$$

The expression for the hysteresis source voltage E_p is written[5] as

$$E_p = j(X_{go} + X_p)\, 2\sqrt{2}\,\frac{r_h H_c}{m N_s} \cdot \left(\frac{P}{2}\right) J\angle -\beta' \text{ volts (rms)} \qquad (59)$$

where J is a factor. It expresses fundamental solution of Fourier Series of flux space wave and β' is the angle between Thevenin equivalent magnetic potential $F_{q\theta}$ and ϕ_θ .

2. GENERAL EQUIVALENT CIRCUIT.

In the analysis of equivalent circuit models of practical hysteresis machines at synchronous mode of operation an usual approach is to either neglect saturation or to use only one saturable reactance. But economic consideration require operation of the machine in the magnetically saturated region and when the stator core becomes saturated, the single reactance is not sufficient to represent the stator reactance adequately.

For accurate representation of the stator saturation Slemon[18] tried to determine the different regions of magnetic saturation of the stator and to identify the magnetic flux variable on which the saturation in each region depends. From that analysis it was concluded that the stator reactance X_s may be replaced by the reactances X_{sa}, X_{sb} and X_{ty} of the different saturating regions, where X_{sa} represents the end winding reactances, X_{sb} the slot, tooth top and zig-zag reactances and X_{ty} the tooth body and yoke reactance.

It has been shown[18] that the tooth body saturation is caused by the vector sum of airgap flux density and the tooth body leakage flux density. The airgap flux density B_1 links with the stator winding to produce the airgap voltage E_g . The flux density component B_t links with the stator winding to produce the leakage reactance voltage $jX_{sb} I_s$. The space vector sum of the two flux density

distribution links with the stator winding to produce the voltage E_{ty}. The voltage E_{ty} differs from the stator terminal voltage only by the voltage induced by the normally small and winding leakage flux and the resistance drop. This same voltage E_{ty} represents the flux in the yoke. The magnetomotive force required for the stator tooth-body and the yoke may now be represented as the magnetizing current I_{ty} through the reactance X_{ty} connected across the voltage E_{ty}. The value of the reactance X_{ty} is a function of the voltage E_{ty} only. This is shown in the Fig.16.

In the previous analysis of parasitic loss, the mmf-parasitic loss component is shown to be directly proportional to the square of the r.m.s. stator current i.e.,

$$P_m = K_m I_s^2 \qquad (18)$$

Where K_m is the mmf - loss constant and I_s is the r.m.s. stator current. Thus the mmf - parasitic loss may conveniently be represented by an equivalent resistance R_m which is numerically equal to K_m.

Similarly, the flux-parasitic loss is shown to be proportional to the square of the airgap voltage. For sinusoidal space flux density wave for, this loss component P_f is denoted as

$$P_f = K'_f E_g^2 \qquad (30)$$

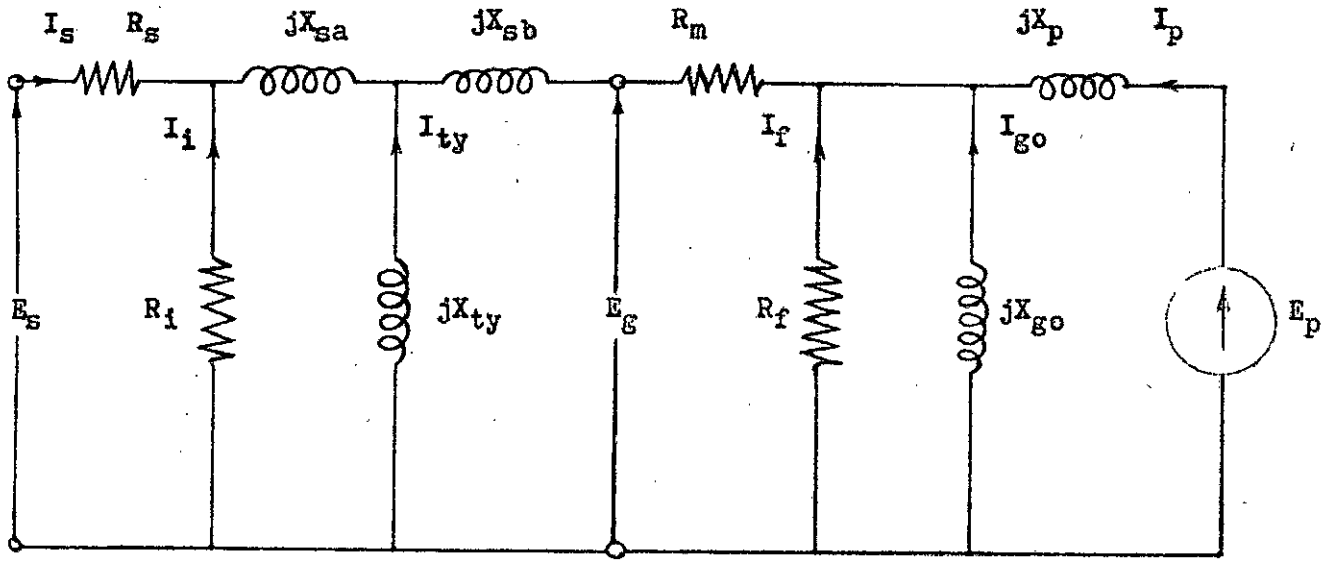

Fig.16. General Equivalent Circuit of Hysteresis Machine — Synchronous Mode.

where K'_f is the flux - loss constant and E_g is the airgap voltage. Thus the flux-parasitic loss may also be represented by an equivalent resistance R_f which depends on the airgap voltage and is numberically equal to the reciporocal of the flux-loss constant K'_f . This is shown in Fig.16.

The representation of the stator iron loss R_i between R_s and X_s in the equivalent circuit of Fig.16 is claimed to be more accurate than the classical representation.

Considering all the above assumptions the general equivalent circuit for a practical hysteresis machine operated at synchronous speed is shown in Fig.16.

3. ANALYTICAL SOLUTION OF GENERAL EQUIVALENT CIRCUIT.

The phasor quantities of the general equivalent circuit (Fig. 16) of the hysteresis machine for synchronous mode of operation may be expressed by phasor equations. Using loop method, we get

$$E_s = I_s R_s - I_i R_i \tag{60}$$

$$0 = I_i R_i + (I_s + I_i) jX_{sa} - I_{ty} jX_{ty} \tag{61}$$

$$0 = I_{ty} jX_{ty} + (I_s + I_i + I_{ty})(R_m + jX_{sb}) - I_f R_f \tag{62}$$

$$0 = I_f R_f - I_{go} jX_{go} \tag{63}$$

$$-E_p = I_{go} jX_{go} - I_p jX_p \tag{64}$$

From Fig.16, $-I_{go} = I_s + I_i + I_{ty} + I_f + I_p$ (65)

From eqn.(61), $- I_i R_i = (I_s + I_i) jX_{sa} - I_{ty} jX_{ty}$ (66)

From eqn.(62), $- I_{ty} jX_{ty} = (I_s + I_i + I_{ty})(R_m + jX_{sb}) - I_f R_f$ (67)

From eqn.(63), $- I_f R_f = - I_{go} jX_{go}$ (68)

Using the values from eqns. (65),(66),(67) and (68)

we get,

From eqn.(60),

$$E_s = I_s R_s + (I_s + I_i) jX_{sa} + (I_s I_i + I_{ty}) + (R_m + jX_{sb}) + (I_s + I_i + I_{ty} + I_f + I_p) jX_{go}$$

$$= I_s \left[(R_s + R_m) + j(X_{sa} + X_{sb} + X_{go}) \right] + I_i \left[R_m + j(X_{sa} + X_{sb} + X_{go}) \right] + I_{ty} \left[R_m + j(X_{sb} + X_{go}) \right] + I_f jX_{go} + I_p jX_{go} \quad (69)$$

From eqn.(61),

$$0 = I_i R_i + (I_s + I_i) jX_{sa} + (I_s + I_i + I_{ty}) (R_m + jX_{sb}) + (I_s + I_i + I_{ty} + I_f + I_p) jX_{go}$$

$$= I_s \left[R_m + j(X_{sa} + X_{sb} + X_{go}) \right] + I_i \left[(R_i + R_m) + j(X_{sa} + X_{sb} + X_{go}) \right] + I_{ty} \left[R_m + j(X_{sb} + X_{go}) \right] + I_f jX_{go} + I_p jX_{go} \quad (70)$$

From eqn.(62),

$$0 = I_{ty} jX_{ty} + (I_s + I_i + I_{ty}) (R_m + jX_{sb}) + (I_s + I_i + I_{ty} + I_f + I_p) jX_{go}$$

$$= I_s \left[R_m + j(X_{sb} + X_{go})\right] + I_i \left[R_m + j(X_{sb} + X_{go})\right] + I_{ty} \left[(R_m + j(X_{ty} + X_{sb} + X_{go})\right] + I_f \, jX_{go} + I_p \, jX_{gp} \quad (71)$$

From eqn.(63),

$$0 = I_f R_f + (I_s + I_i + I_{ty} + I_f + I_p) jX_{go}$$

$$= I_s \, jX_{go} + I_i \, jX_{go} + I_{ty} \, jX_{go} + I_f (R_f + jX_{go}) + I_p \, jX_{go} \quad (72)$$

From eqn. (64),

$$E_p = (I_s + I_i + I_{ty} + I_f + I_p) jX_{go} + I_p \, jX_p$$

$$= I_s \, jX_{go} + I_i \, jX_{go} + I_{ty} jX_{go} + I_f \, jX_{go} + I_p j(X_{go} + X_p) \quad (73)$$

Thus the phasor equations for the general equivalent circuit may be written in the matrix form from eqnx.(69) through (73) as

$$
\begin{bmatrix} E_s \\ 0 \\ 0 \\ 0 \\ E_p \end{bmatrix} = \begin{bmatrix} (R_s + R_m) + j(X_{sa} + X_{sb} + X_{go}) & R_m + j(X_{sa} + X_{sb} + X_{go}) & R_m + j(X_{sb} + X_{go}) & jX_{go} & jX_{go} \\ R_m + j(X_{sa} + X_{sb} + X_{go}) & (R_i + R_m) + j(X_{sa} + X_{sb} + X_{go}) & R_m + j(X_{sb} + X_{go}) & jX_{go} & jX_{go} \\ R_m + j_b(X_{sb} + X_{go}) & R_m + j(X_{sb} + X_{go}) & R_m + j(X_{ty} + X_{sb} + X_{go}) & jX_{go} & jX_{go} \\ jX_{go} & jX_{go} & jX_{go} & R_f + jX_{go} & jX_{go} \\ jX_{go} & jX_{go} & jX_{go} & jX_{go} & j(X_{go} + X_p) \end{bmatrix} \begin{bmatrix} I_s \\ I_i \\ I_{ty} \\ I_f \\ I_p \end{bmatrix} \quad (74)
$$

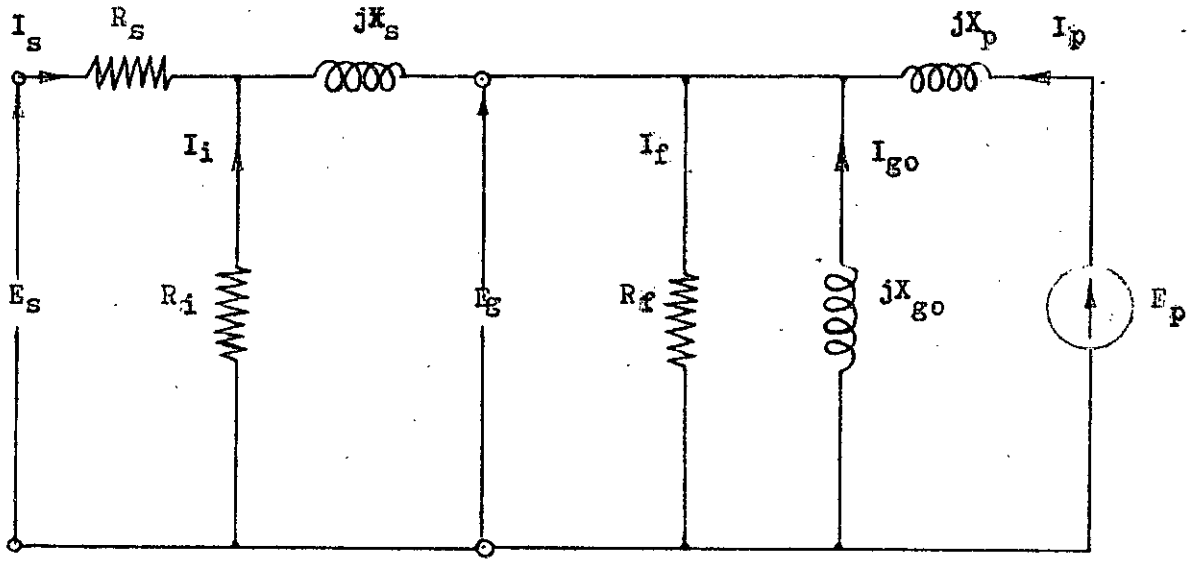

Fig.17. Modified General Equivalent Circuit for Synchronous Mode of Operation.

4. MODIFIED EQUIVALENT CIRCUIT

In an integral horse-power hysteresis machine having higher number of slots per pole per phase, the flux-parasitic loss is the predominent component representing approximately 80% of the total parasitic loss. Under such situations the resistance R_m representing the mmf - parasitic loss in the general equivalent circuit may be ignored.

If the machine is operated at low terminal voltage such that the stator saturation effect is neglected, the ractance X_{ty} being small is negligible and thus the reactance X_s is the sum of the series reactances X_{sa} and X_{sb}. The modied equivalent circuit is shown in Fig. 17.

5. ANALYTICAL SOLUTION OF MODIFIED EQUIVALENT CIRCUIT.

For the mathematical solution of the modified general equivalent circuit, let us use the loop method. The loop equations are:

$$E_s = I_s R_s - I_i R_i \tag{75}$$

$$0 = I_i R_i + (I_s + I_i) jX_s - I_f R_f \tag{76}$$

$$0 = I_f R_f - I_{go} jX_{go} \tag{77}$$

$$-E_p = I_{go} jX_{go} - I_p jX_p \tag{78}$$

From Fig. 17,

$$-I_{go} = I_s + I_i + I_f + I_p \tag{79}$$

From eqn.(76),

$$-I_i R_i = (I_s + I_i)\, jX_s - I_f R_f \tag{80}$$

From eqn.(77),

$$-I_f R_f = -I_{go} jX_{go} \tag{81},$$

Substituting the values from eqn.(79),(80) and (81),

we get,

From eqn.(75),

$$E_s = I_s R_s + (I_s + I_i)\, jX_s + (I_s + I_i + I_f + I_p)\, jX_{go}$$

$$= I_s \left[R_s + j(X_s + X_{go})\right] + I_i\, jX(X_s + X_{go}) + I_f\, jX_{go} + I_p\, jX_{go} \tag{82}$$

From eqn.(76),

$$0 = I_i R_i + (I_s + I_i)\, jX_s + (I_s + I_i + I_f + I_p)\, jX_{go}$$

$$= I_s\, j(X_s + X_{go}) + I_i \left[R_i + j(X_s + X_{go})\right] + I_f\, jX_{go} + I_p\, jX_{go} \tag{83}$$

From Eqn.(77),

$$0 = I_f R_f + (I_s + I_i + I_f + I_p)\, jX_{go}$$

$$= I_s\, jX_{go} + I_i\, jX_{go} + I_f\, (R_f + jX_{go}) + I_p\, jX_{go} \tag{84}$$

From Eqn.(78),

$$E_p = (I_s + I_i + I_f + I_p)\, jX_{go} + I_p\, jX_p$$

$$= I_s\, jX_{go} + I_i\, jX_{go} + I_f\, jX_{go} + I_p\, j(X_{go} + X_p) \tag{85}$$

Thus the phaser equations of the modified general equivalent circuit of hysteresis machine at synchronous mode of operation may be written in the metrix form as

$$\begin{bmatrix} E_s \\ 0 \\ 0 \\ E_p \end{bmatrix} = \begin{bmatrix} R_s + j(X_s + X_{go}) & j(X_s + X_{go}) & jX_{go} & jX_{go} \\ j(X_s + X_{go}) & R_i + j(X_s + X_{go}) & jX_{go} & jX_{go} \\ jX_{go} & jX_{go} & R_f + jX_{go} & jX_{go} \\ jX_{go} & jX_{go} & jX_{go} & j(X_{go} + X_p) \end{bmatrix} \begin{bmatrix} I_s \\ I_i \\ I_f \\ I_p \end{bmatrix} \quad (86)$$

CHAPTER IV

1. SUB-SYNCHRONOUS MODE.

So far the analysis was restricted to synchronous mode of operation of the hysteresis machine. It was shown that at synchronous speed the motor torque is entirely due to the hysteresis effect. However, at speeds other than the synchronous one the motor torque is due to both hysteresis and eddy current effects. The eddy current torque at speeds other than the synchronous one contributes directly to the total motor torque. Eddy current torque is also important even in the synchronous mode of operation for damping out the huntings[19] of the hysteresis rotor.

To analyse the hysteresis machine for sub-synchronous mode of operation the idealized hysteresis material in the rotor assembly with its complete magnetic synmetry may be represented by a set of balanced polyphase closed windings[11] and hence closed coils having stator to rotor turns ratio of 1:1. In normal induction motor the rotor ressistance is independant of slip and is primarily determined by the winding resistance However, in the case of hysteresis machine at sub-synchronous speed, these coils may be modelled to have both the eddy current dependant resistance R_e and the hysteresis resistance R_h. Unlike the induction motor, the hysteresis resistance R_h is slip dependant.

Derivation of R_h

The hysteresis resistance R_h may be evaluated from the power loss approach. Using the parallelogram approximation as shown in Fig.8 of the actual hysteresis loop of the rotor material, the hysteresis energy W_h per unit volume is

$$W_h = 4B_r H_c \quad \text{Joules} \qquad (87)$$

and the synchronous watts derived from this hysteresis loss may be expressed as

$$P_h = Vf\ W_h = \frac{m\ E_g^2}{R_h} \quad \text{Watts} \qquad (88)$$

where V is the volume of the hysteresis ring and from Fig.11

$$V = 2\pi r_h\ hl. \qquad (89)$$

Thus, from eqns(87), (88) and (89), we get,

$$R_h = \frac{m\ E_g^2}{8\pi r_h\ hlf\ B_f\ H_c} \quad \text{ohms} \qquad (90)$$

Now $$E_g = 4.44\ f\ N\ \phi\ K_w \quad \text{volts} \qquad (91)$$

Where K_w is the winding factor. Thus

$$R_h = \frac{1.11\ m\ f\ N^2 \phi^2 K_w}{2\pi r_h\ hl\ B_r\ H_c} \quad \text{ohms} \qquad (92)$$

This R_h will produce the total synchronous hysteresis watts at all values of slip and at the pull-out condition. The portion(1-S) of this power will appear as mechanical output. This is shown in Fig.19.

Derivation of R_e

To derive the equivalent eddy current resistance R_e, it is not possible to use direct calculation based on physical shape and material resistivity as the hysteresis motor does not have a lear distinction between current carrying and flux carrying rotor members. The power loss approach

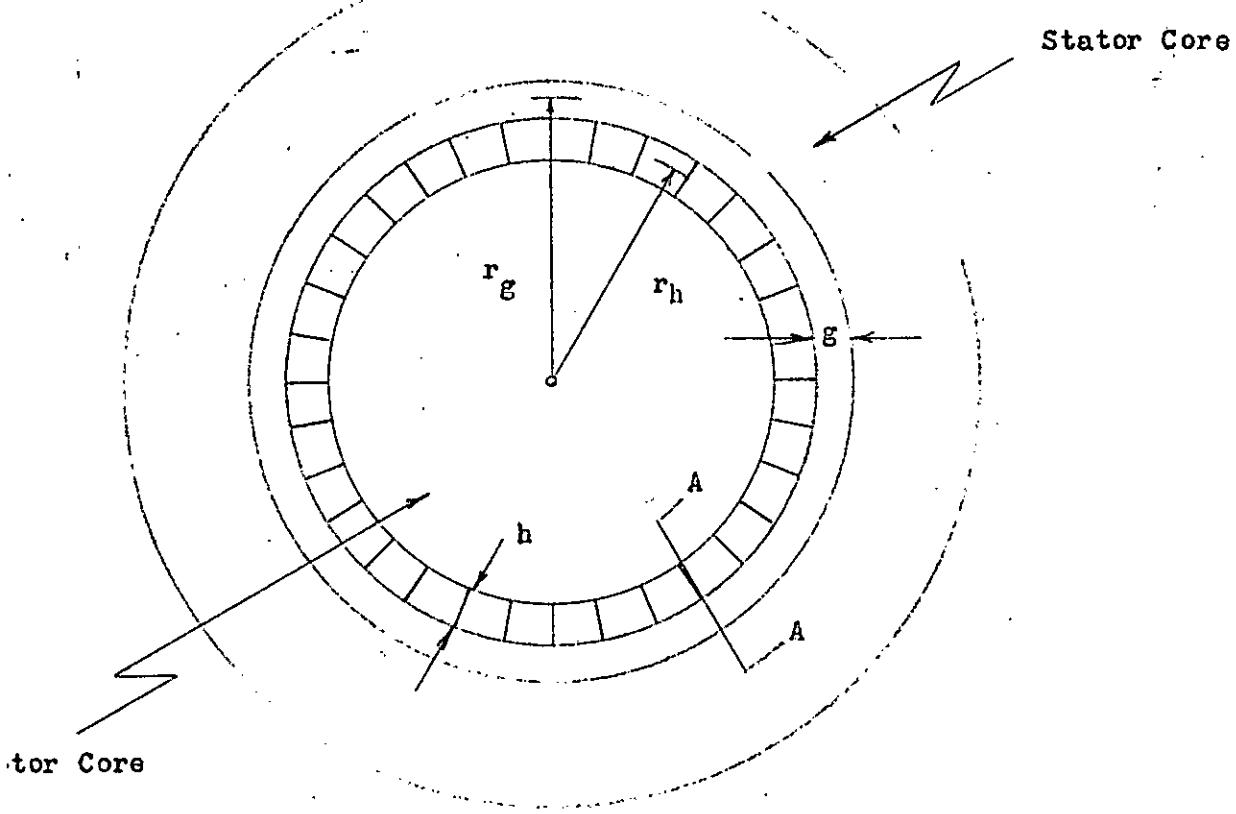

(a)

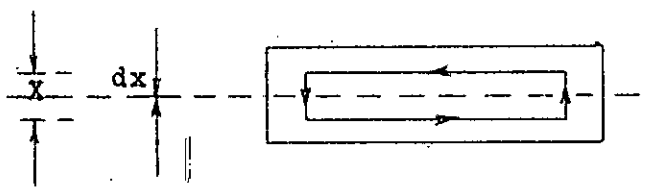

(b)

Fig.18 (a) Cross-Section of Circumferential Flux Hysteresis Machine.

(b) Section A - A of the Rotor Ring.

as used in the case of the hysteresis resistance R_h seems promissing to derive R_e . Thus

$$R = \frac{E_r^2}{P_e} \quad \text{ohms} \qquad (93)$$

where E_r is the rotor induced voltage.

To derive the eddy current loss P_e , let the ring is cut at section A-A,Fig.18(a) and laid out flat as shown in Fig.18(b). If the flux is directed into the paper on the section view, eddy-currents will flow as shown by arrow in the section A-A,Fig.18(b). The magnitude of the current will be determined by the induced voltage and resistively of the material. Considering an incremental thickness dx of the ring at distance X from the mean diameter $2 r_h$, the total resistance experienced by the incremental current through dx will be

$$d R = \frac{\rho l}{\pi r_h \, dx} \qquad (94)$$

Since the incremental current enclosed the portion $2 X/h$ of the total flux, Fig.18(b) in the hysteresis ring, the induced voltage is given by

$$E_r = 4.44 \; f_r \; \phi_h \; (2 X/h) \quad \text{volts} \qquad (95)$$

Where ϕ_h is the peak value of the total circumferential flux assumed to be uniformly distributed in the ring.

Thus the total eddy current loss in watts is

$$P_e = \int_0^{h/2} d P_e$$

$$= \int_0^{h/2} \frac{E_r^2}{d R_e} \qquad (96)$$

Substituting equations (94) and (95) in eqn. (96), we get,

$$P_e = \frac{78.45\pi f_r^2 \phi_h^2 r_h}{\rho 1 h^2} \int_0^{h/2} X^2 \, dx \qquad (97)$$

and after integration,

$$P_e = \frac{10.32 f_r^2 \phi_h^2 r_h h}{\rho 1} \quad \text{watts} \qquad (98)$$

In terms of the stator frequency f, the eddy current loss per phase in the hysteresis motor is

$$P_e = \frac{S^2 E_g^2}{R_e}$$

$$= \frac{10.32 (Sf)^2 \phi_h^2 r_h h}{m \rho 1} \quad \text{watts} \qquad (99)$$

Substituting the value of E_g in eqn.(99), we get the expression for the eddy current resistance R_e as

$$R_e = \frac{1.9\ N^2\ m\ \rho\ l}{r_h\ h} \quad \text{ohms} \qquad (100)$$

2. EQUIVALENT CIRCUITS.

The equivalent circuit of the hysteresis machine at sub-synchronous mode of operation is shown in Fig.19. Fig.20 shown a general equivalent circuit for sub-synchronous mode of operation including the stator iron losses and parasitic losses. These equivalent circuits models of Fig.19 and 20 holds good for any speed except the synchronous one. At synchronous speed with $S = 0$ the eddy current element is absent and the hysteresis element may be conveniently replaced by a constant source of voltage E_p as shown in Fig.14.

It may be mentioned here that the phasor quantities shown in Figs.19. and 20 in the case of sub-synchronous mode of operation will be somewhat different from that in the case of synchronous mode of operation. Since there does not exist any definite procedure in practice for the calculation of these quantities, it is really difficult to find out the exact values. Thus for simplicity these phasor quantities were assumed constant for all speeds.

For sub-synchronous mode at slip S, the perphase $I^2 R$ loss in the rotor hysteresis ring, neglecting the minor loop losses, is

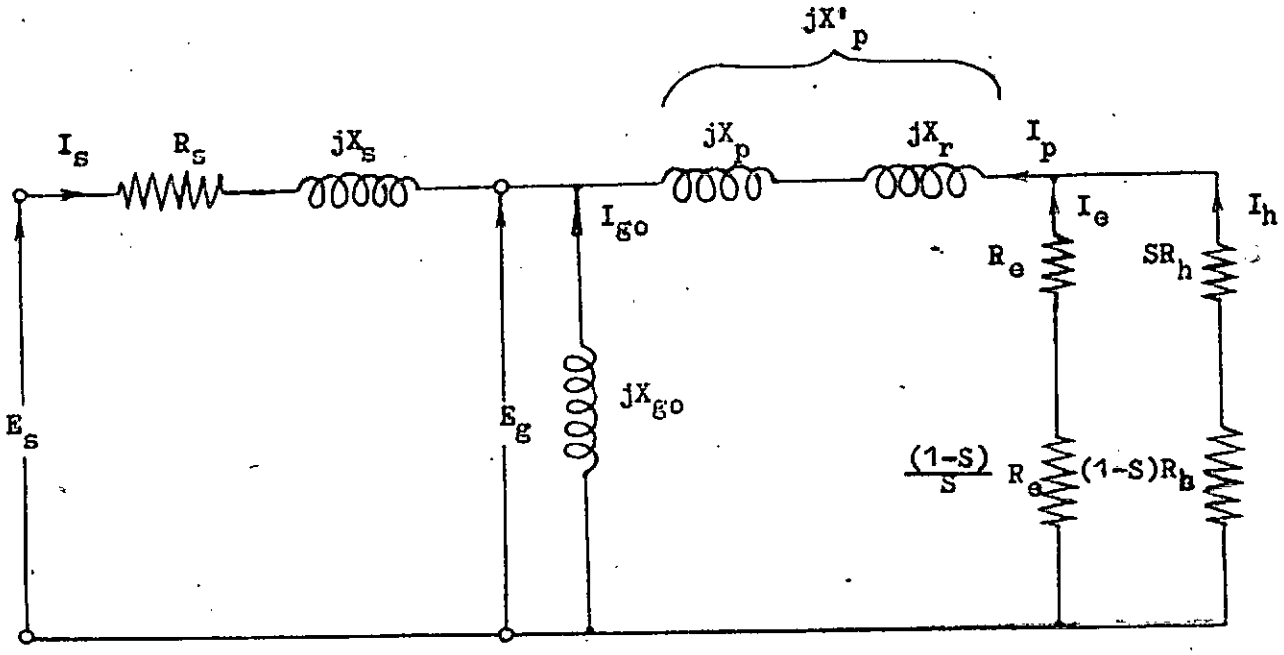

Fig.19. Equivalent Circuit for Sub-Synchronous Mode of Operation.

$$P_c = I_e^2 R_e + I_h^2 \, S \, R_h \qquad \text{Watts} \qquad (101)$$

The output power per phase is

$$P_o = I_e^2 \left(\frac{1 - S}{s}\right) R_e + I_h^2 (1-S) R_h \quad \text{watts} \qquad (102)$$

This is shown in Fig.(19) and (20). The first terms in eqn.(101) and (102) show the contribution due to eddy current, while the second terms represent the contribution due to the hysteresis effects.

3. ANALYTICAL SOLUTION OF EQUIVALENT CIRCUIT.

From Fig. 19, the loop equations are

$$E_s = I_s (R_s + jX_s) - I_{go} jX_{go} \qquad (103)$$

$$0 = I_{go} jX_{go} - I_p jX'_p - I_e \left(R_e + \frac{1-S}{S} R_e\right) \qquad (104)$$

where $X'_p = X_p + X_r$, (105)

X_r , being the rotor leakage reactance.

$$0 = I_e R_e + \frac{1 - S}{S} R_e) - I_h SR_h + (1 - S) R_h \qquad (106)$$

From Fig.19,

$$I_p = I_e + I_h \qquad (107)$$

$$\text{and} \quad -I_{go} = I_s + I_p + I_s + I_e + I_h \qquad (108)$$

From eqn.104,

$$-I_e \left(R_e + \frac{1-S}{S} R_e\right) = I_{go}\, jX_{go} - I_p\, jX'_p$$

$$= (I_s + I_e + I_h)\, jX_{go} + (I_e + I_h)\, jX'_p \qquad (109)$$

Using the eqns.(107),(108) and (109), we get,

From eqn. (103),

$$E_s = I_s (R_s + jX_s) + (I_s + I_e + I_h)\, jX_{go}$$

$$= I_s \left[R_s + j(X_s + X_{go})\right] + I_e\, jX_{go} + I_h\, jX_{go} \qquad (110)$$

From eqn.(104),

$$0 = (I_s + I_e + I_h)\, jX_{go} + (I_e + I_h)\, jX'_p + I_e\, 1/S\, R_e$$

$$= I_s\, SjX_{go} + I_e \left[R_e + jS(X_{go} + X'_p)\right] + I_h\, jS(X_{go} + X'_p) \qquad (111)$$

From eqn.(106),

$$0 = (I_s + I_e + I_h)\, jX_{go} + (I_e + I_h)\, jX'_p + I_h\, SR_h + (1 - S)\, R_h$$

$$= I_s\, jX_{go} + I_e\, j(X_{go} + X'_p) + I_h \left[R_h + j(X_{go} + X'_p)\right] \qquad (112)$$

Multiplying throughout by S, we get

$$0 = I_s\, SjX_{go} + I_e\, Sj(X_{go} + X'_p) + I_h\left[SR_h + jS(X_{go}+X'_p)\right] \qquad (113)$$

Thus the phasor equations of the equivalent circuit of hysteresis machine at sub-synchronous mode of operation may be written in the matrix for as

$$\begin{bmatrix} E_s \\ 0 \\ 0 \end{bmatrix} = \begin{bmatrix} R_s + j(X_s + X_{go}) & jX_{go} & jX_{go} \\ jSX_{go} & R_e + jS(X_{go}+X'_p) & JS(X_{go}+X'_p) \\ jSX_{go} & jS(X_{go}+X'_p) & SR_h + jS(X_{go}+X'_p) \end{bmatrix} \begin{bmatrix} I_s \\ I_e \\ I_h \end{bmatrix} \qquad (114)$$

4. ANALYTICAL SOLUTION OF GENERAL EQUIVALENT CIRCUIT.

From Fig. 20, the loop equations are:

$$E_s = I_s R_s - I_i R_i \qquad (115)$$

$$0 = I_i R_i + (I_s + I_i)\, jX_s - I_f R_f \qquad (116)$$

$$0 = I_f R_f + I_{go} jX_{go} \qquad (117)$$

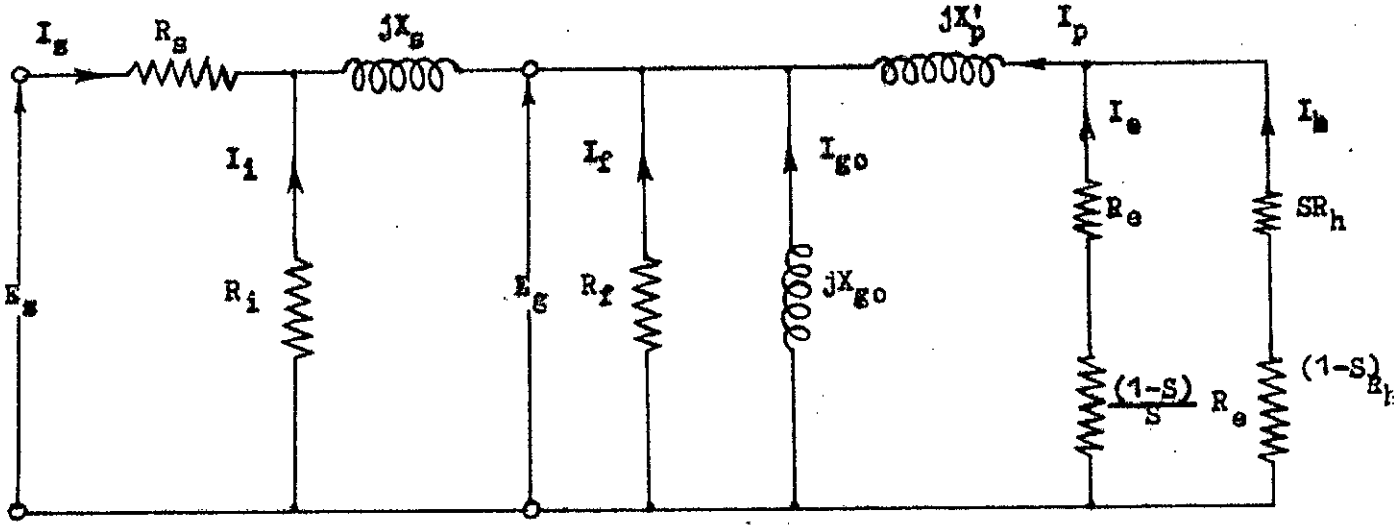

Fig.20. General Equivalent Circuit at Sub-Synchronous Mode of Operation.

$$0 = I_{go} jX_{go} - I_p jX'_p - I_e \left(R_e + \frac{1 - S}{S} R_e \right) \quad (118)$$

$$0 = I_e \left(R_e + \frac{1 - S}{S} R_e \right) - I_h \left[SR_h + (1 - S) R_h \right] \quad (119)$$

From Fig. 20,

$$I_p = I_e + I_h \quad (120)$$

$$- I_{go} = I_s + I_i + I_f + I_e + I_h \quad (121)$$

From eqn. (116),

$$= I_i R_i = (I_s + I_i) jX_s - I_f R_f \quad (122)$$

From eqn.(117)

$$- I_f R_f = - I_{go} jX_{go} \quad (123)$$

From eqn.(118)

$$- I_e \left(R_e + \frac{1 - S}{S} R_e \right) = - I_{go} jX_{go} + I_p jX'_p \quad (124)$$

Using the eqns.(120) through (124) we get,

From eqn. (115),

$$E_s = I_s R_s + (I_s + I_i) jX_s + (I_s + I_i + I_f + I_e + I_h) jX_{go}$$

$$= I_s \left[R_s + j(X_s + X_{go}) \right] + I_i j(X_s + X_{go}) + I_f jX_{go} + I_e jX_{go} + I_h jX_{go} \quad (125)$$

From eqn. (116)

$$0 = I_i R_i + (I_s + I_i) jX_s + (I_s + I_i + I_f + I_e + I_h) jX_{go}$$

$$= I_s j(X_s + X_{go}) + I_i [R_i + j(X_s + X_{go})] + I_f jX_{go} + I_e jX_{go} + I_h jX_{go} \quad (126)$$

From eqn.(117),

$$0 = I_f R_f + (I_s + I_i + I_f + I_e + I_h) jX_{go}$$

$$= I_s jX_{go} + I_i jX_{go} + I_f (R_f + jX_{go}) + I_e jX_{go} + I_h jX_{go} \quad (127)$$

From eqn.(118),

$$0 = (I_s + I_i + I_f + I_e + I_h) jX_{go} + (I_e + I_h) jX'_p + I_e R/SR_e$$

$$= I_s SjX_{go} + I_i SjX_{go} + I_f SjX_{go} + I_e [R_e + jS(X_{go} + X'_p)] + I_h jS(X_{go} + X'_p) \quad (128)$$

From eqn.(119),

$$0 = (I_s + I_i + I_f + I_e + I_h) jX_{go} + (I_e + I_h) jX'_p + I_h R_h$$

$$= I_s jX_{go} + I_i jX_{go} + I_f jX_{go} + I_e j(X_{go} + X'_e) + I_h [R_h + j(X_{go} + X'_p)] \quad (129)$$

Multiplying throughout by S, we get

$$0 = I_s jSX_{go} + I_i jSX_{go} + I_f jSX_{go} + I_e jS(X_{go} + X'_p) + I_h [SR_h + JS(X_{go} + X'_p)] \quad (130)$$

Thus the phasor equations of the general equivalent circuit of Fig.20 may be expressed in the matrix form as

$$\begin{bmatrix} E_s \\ 0 \\ 0 \\ 0 \\ 0 \end{bmatrix} = \begin{bmatrix} R_s + j(X_s + X_{go}) & j(X_s + X_{go}) & jX_{go} & jX_{go} & jX_{go} \\ j(X_s + X_{go}) & R_i + j(X_s + X_{go}) & jX_{go} & jX_{go} & jX_{go} \\ jX_{go} & jX_{go} & R_f + jX_{go} & jX_{go} & jX_{go} \\ jSX_{go} & jSX_{go} & jSX_{go} & R_e + jS(X_{go} + X'_p) & jS(X_{go} + X'_p) \\ jSX_{go} & jSX_{go} & jSX_{go} & jS(X_{go} + X'_p) & SR_h + jS(X_{go} + X'_p) \end{bmatrix} \begin{bmatrix} I_s \\ I_i \\ I_f \\ I_e \\ I_h \end{bmatrix} \quad (131)$$

CHAPTER V

1. DISCUSSION

The B-H characteristic of the rotor hysteresis material is a multivalued non-linear function. The area of the loop is dependant on the level of excitation as well as the history, of magnetic material. For different excitation a series of loop is shown in Fig.21. At lower values of excitation, the loop is less rectangular in nature; and for such cases the elliptical modelling may be reasonable. Usually a good hysteresis material has a co-ercieve force lying between 120 - 170 0_e. For such values the parallelogram model may better fit the actual loop.

The treatment of parasitic losses associated with the rotor hysteresis material is a couplex one, as under loaded condition the airgap flux is modified due to stator slotting, winding distribution and saturation in a complex fashion. In the expressions of both the mmf and flux parasitic loss factors K_{mn} and K_f of eqns.(13) and (27) respectively, the influence of recoil permeability μ_r of the minor loops is implied [6]. This value of of μ_r for minor loops is assumed linear and constant for all frequencies. However, the minor loops are distributed on the major loop in a random way. Their recoil permeabilities are neither constant nor colinear. Actually they are non-linear and complex.

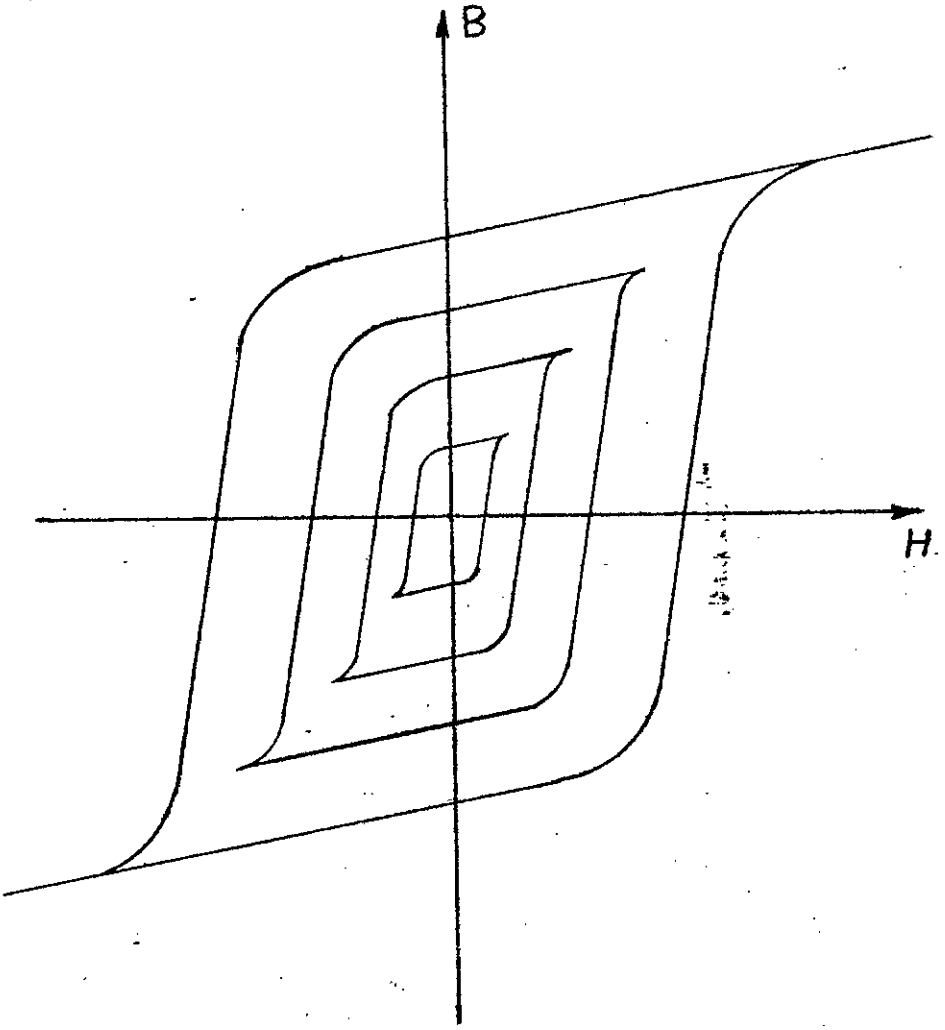

Fig.2.1. B-H Characteristic with Different Level of Excitation.

Although the saturation in the stator is considered adequately for the better representation of the stator reactances, the effect of saturation is neglected in the expressions of parasitic losses. It is however shown[6] that the contribution of stator saturation to the parasitic loss is usually much less significant than the airgap proximity, machine geometry and magneto-electric characteristics of the rotor hysteresis material.

In the derivation of the idealized magnetic equivalent circuit the following equation is implied.

$$F_\theta = - R_g \frac{d^2 \phi_\theta}{d_\theta^2} + R_o \phi + R_p (\phi_\theta - \phi_{p\theta}) \qquad (132)$$

This equation leads to the equivalent circuit of Fig.13 where ϕ_θ is assumed sinusoidal in the airgap. But actually the airgap flux is non-sinusoidal and the term $(- R_g \frac{d^2 \phi_\theta}{d_\theta^2})$ is non-linear. For the purpose of linearizing the airgap reductance, the airgap flux is assumed sinusoidal. For the sinusoidal flux the double differentiation of ϕ_θ with respect to θ results in reversal of sign only i.e., a phase shift of half the period of the flux space wave.

However, it may not be that much accurate and for more elaborate treatment, the equation (132) should be solved numerically.

In the dual electric equivalent circuit, the linearized model of the B-H loop in the magnetic circuit is represented by a constant voltage source E_p . This constant voltage source E_p is an approximation to the actual loop and hence may be a limitation in this work.

Flux parsitic loss factor K_f is voltage dependant and it is represented by a parallel resistance R_f across the airgap while the mmf - parasitic loss factor, K_{mn} is current dependant and it is represented by a resistance R_m in series with the stator impedance in the generatized equivalent circuit of Fig.16. However, the flux parasitic loss relement R_f is put after R_m in the equivalent circuit. Since the loss due to R_f is directly subtracted from the rotor develop power, its representation as given in the equivalent circuit is justified.

The parasitic loss components are frequency dependant as shown in eqns.(13) and (25). At synchronous speed the frequency is constant and the loss components are also constant as shown in Fig.16. But at sub-synchronous speed there results some variation in frequency which in turn causes variation in the loss components.

However, the variation in frequency is not much higher so that the effect of variation in the loss component may be neglected.

At sub-synchronous speed the total torque developed in the rotor is composed of both the eddy current and hysteresis torque. This is shown in Fig.(19) and (20). Of this the element R_e represents $I^2 R$ loss due to eddy current and the element $(\frac{1}{S} - S)R_e$ represents the contribution of the eddy current torque to the output shaft power. Similarly, the element SR_h represents the $I^2 R$ loss due to hysteresis effect and the portion $(1-S)\ R_h$ is the contribution of hysteresis effect to the out put shaft power.

At synchronous speed the slip $S = 0$, and the element $\frac{1-S}{S} R_e$ becomes infinity. This is equivalent to open circuit of the eddy branch. This is consistant with the equivalent circuit analysis of concentional induction motor. However, the $S\ R_h$ element of the hysteresis branch becomes short circuited at $S \neq 0$, and the out put shaft power element due to hysteresis reduces to R_h. Thus the out put torque only comes entirely out of the hysteresis effect. This hysteresis element at synchronous speed is conveniently expressed [4-5] as E_p in Fig.16. The justification of connecting the eddy element with the hysteresis element in parallel is clearly spelt out in the aforesaid discussions.

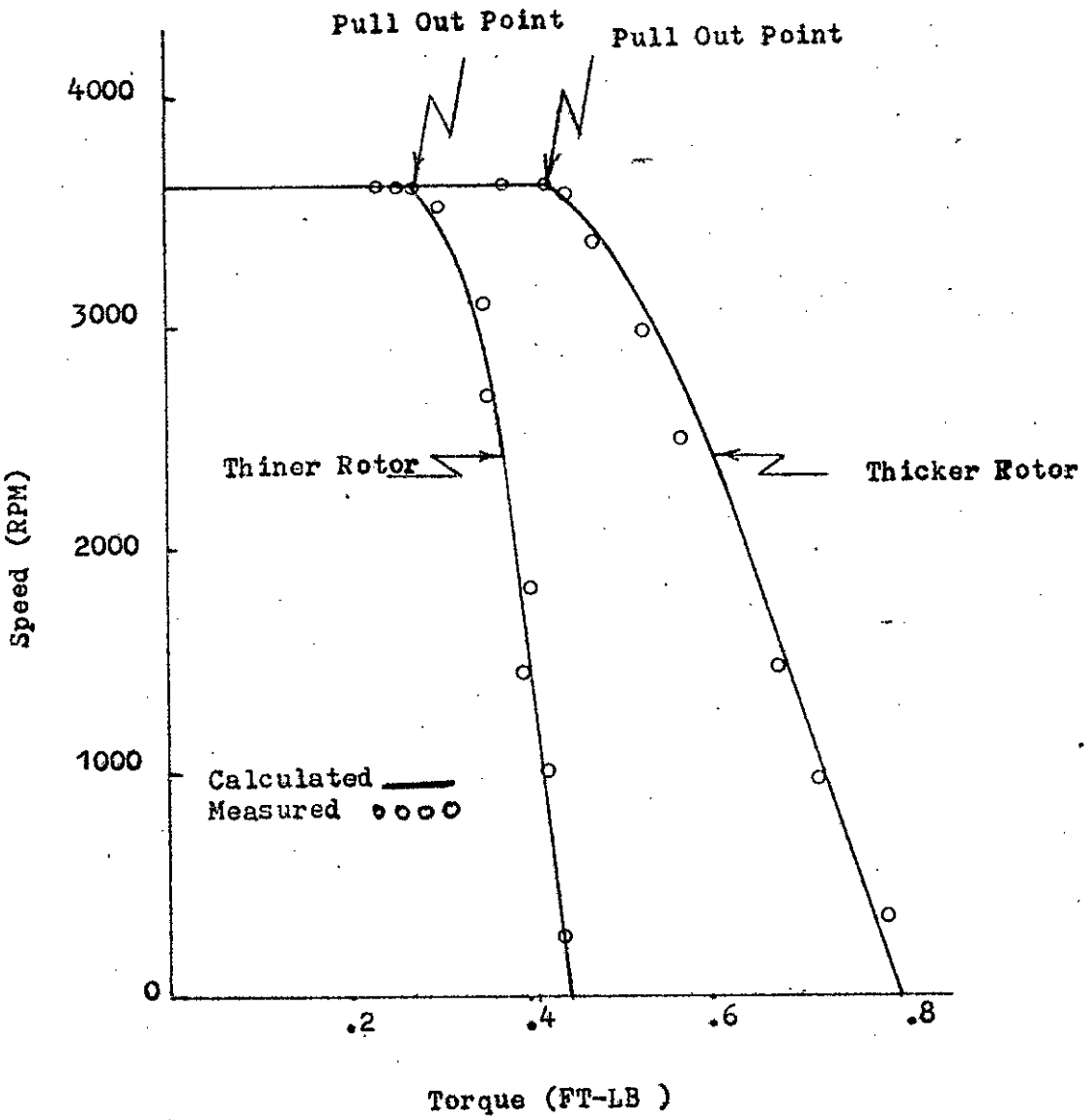

Fig.22. Speed Torque Characteristics.

Fig.22 shows the experimental [10] speed torque curve of synchronous hysteresis motor with two types of rotor, namely thicker and thiner rotors. Upto synchronous speed both the speed-torque curves are ideally flat. However, at sub-synchronous speed the torque for both types of rotor are greater than the corresponding pull out torque at synchronous speed. Thus, it is evident from Fig.22 that the torque at sub-synchronous speed is higher than the synchronous pull-out torque. At synchronous speed the total machine developed power is $I_h^2 R_h$ as implied in Figs.(19) and (20). At sub-chronous speed the output shaft power is

$$P_o = I_h^2 (1-S) R_h + I_e^2 \left(\frac{1-S}{S}\right) R_e \qquad (102)$$

From the experimental torque - speed curve of Fig.22, it is to be noted that

$$I_h^2 (1-S) R_h + I_e^2 \left(\frac{1-S}{S}\right) R_e > I_h R_h \qquad (133)$$

even though there exists $I_e^2 R_e$ loss in both the elements namely $I_e^2 R_e$ and $I_h^2 S R_h$. This is in agreement with our prediction in the equivalent circuit of Fig.22 that at sub-synchronous speed the eddy current torque contributes to the total machine torque. The additional torque above the pull-out one is due to the resultant eddy current.

2. CONCLUSIONS

General equivalent circuit models for polyphase hysteresis motors are derived. Corresponding solutions of these equivalent circuits in phasor quantities are obtained. A detail investigation into the phenomena of stator saturation, parasitic losses and iron losses have been made. These effects are represented by appropriate parameters in the equivalent circuit models. The equivalent circuit models for both synchronous and sub-synchronous mode of operation are also developed. Modified equivalent circuit models for both the cases are obtained. These equivalent circuit models are suitable for sleady state operation.

The analytical solutions are rigorous and reasonably complete for a balanced polyphase hysteresis motor.

At sub-synchronous speed it is established that the additional torque over the pull-out one is due to the eddy current torque. This is found in agreement with that obtained experimentally.

Further work may be done on the optimum design of hysteresis motor based on the parameters developed in this analysis. More detailed experimental investigations particularly at the sub-synchronous mode of operation of the motor should be carried out in future work.

REFERENCES

1. C.P.Stienmetz,"Theory and Calculation of Electrial Apparatus" (book), Mc Graw-Hill, New York, 1917.
2. B.R. Teare, "Theory of Hysteresis Motor Torque",A.I.E.E.Transactions, vol.59, 1940, pp.907-12.
3. R.C.Roters, "The Hysteresis Motor-Advances which Permit Economical Fraction Horse Power Rating", A.I.E.E. Transactions, vol.66,1947, pp.1419 - 1430.
4. M.A.Copeland and G.R.Slemon,"An Analysis of the Hysteresis Motor: I - Analysis of the idealized Machine", I.E.E.E.Transactions,Power Apparatus and Systems, vol.82,April 1962, pp.34 - 42.
5. M.A.Copeland and G.R.Slemon," An Analysis of the Hysteresis Motor: II - The Circumferential - flux Machine," I.E.E.E. Transactions,Power Apparatus and Systems, vol.83,June, 1964, pp.619 - 625.
6. M.A.Rahman, M.A.Copeland and G.R.Slemon",An Analysis of the Hysteresis Motor Part-III : Parasitic Losses," I.E.E.E. Transactions, Power Apparatus and Systems, vol.88,No.6,June, 1969,pp.954 - 61.
7. M.A.Rahman,"Minor Loop Losses in Hysteresis Torque Devices Using permanent Magnet Material", I.E.E.E. Transactions on Magnetics,New York, vol.Mag. - 6,No.3,Sept. 1970, pp.474.
8. M.A.Rahman,"The Electrification of Irrigation Projects in Bangladesh", the Proceedings of Power Seminer,BUET,Dacca,May 21, 1972.
9. M.A.Rahman,"Use of Synchronous Hysteresis Motor in Low Lift Power Pumps", Journal, I.E.Bangladesh (Pakistan) vol.9,No.12,convension issue, Dec., 1969, pp.607 -609.

10. M.A.Rahman,"Design of Hysteresis Motor", Journal,I.E.Bangladesh (Pakistan) vol.10, No.12,convention Issue, Dec.1970,pp.1205 -1210.

11. M.A.Rahman,"Analytical Models for Poly phase Hysteresis Motor", I.E.E.E. Transactions, Power Apparatus and Systems, New York, vol.PAS-92,No.1,Jan - Feb.1973,pp.237 - 242.

12. S.Miyairi and T.Kataoka, "A Basic Equivalent Circuit of the Hysteresis Motor", Journal I.E.E.,Japan,vol.85, 1965,pp.41 - 50.

13. M.A. Copeland and G.R.Slemon,"Minor Loop Loss Prediction in Devices Using Permanent Magnet Materials", I.E.E.E. Transactions on Magnetics, vol.Mag.- 2,pp.420 -423 , Sept. 1966.

14. P.H. Trickey," Iron-Loss Calculation on Fractional Horse Power Induction Motor,"I.E.E.E. Transactions, Power Apparatus and Systems, vol.76, Part 3, 1958, pp. 1963 - 1969.

15. D.O 'Kelly, "Equivalent circuits for single Phase Induction and Hysteresis Motors", I.E.E.E. Transactions Paper No. 70T -P9-PWR, Winter Power Meeting,New York, 1970.

16. R.C.Parker and R.J.Studders,"Permanent Magnets and their Applications" (book), Wiley, New York, 1963.

17. G.R.Slemon,"Magneto-Electric Devices",(book),Wiley,New York,1966.

18. G.R.Slemon,"Analytical Models for Saturated Synchronous Machines", I.E.E.E. Transactions Paper No.70T -P535-PWR,Summer Power Meeting, Los Angeles, 1970.

19. S.P.Clurman,"On Hunting in Hysteresis Motors and New Damping Technique", I.E.E.E., Transaction on Magnetics,vol.Mag.7,No.3 Sept. 1971, pp. 512-517.

20. S. Miyairi and T.Kataoka,"Analysis of Hysteresis Motors considering Eddy Current Effects", Journal I.E.E., Japan,vol.86, 1966,pp.67 - 77.

21. G.Wakui and Y.Kusakari," Synchronous Pull-out of Hysteresis Motor", Journel I.E.E., Japan,vol.85, 1965, pp.1044 - 53.

22. G.Wakui, "Optimum Conditions in Design of Hysteresis Motor",Journel I.E.E., Japan, vol.86, No.II,November, 1966, pp. 95 - 105.

23. P. Walker, "A Method for Designing and Analyzing Hysteresis Motor", I.E.E.E. conference Paper No.68C-P36 - PWR, Winter Power Meeting, New York, 1968.

24. S.D.T.Robertson and S.Z.G.Zaky, "Analysis of the Hysteresis Machine - Part -I", I.E.E.E. Transactions, Power Apparatus and Systems, vol.88,April, 1969, pp.474 - 483.

25. T.Takahashi,"Calculation of Rotor Import Power for Hysteresis Motor Running at synchronous speed", Journel I.E.E.,Japan,vol.89,No.7, 1969, pp.78 - 87.

26. P.L.Alger,G.Angst and W.M. Schweder,"Saturistors and Low Starting Current Induction Motor", I.E.E.E.Transactions,Power Apparatus and Systems,vol.81,June 1963,pp.291 -298.